Ephrin-B1 and EphB4 as novel markers for steroidogenic cells in naturally cycling mouse ovary and adrenal gland

大阪府立大学博士（獣医学）学位論文

Ephrin-B1 and EphB4 as novel markers for steroidogenic cells in naturally cycling mouse ovary and adrenal gland

（自然発情周期下のマウスの卵巣と副腎のステロイド産生細胞における
新規マーカー分子 ephrin-B1 と EphB4）

JAHAGIR ALAM

2022 年

Contents

General introduction

Erythropoietin-producing hepatocellular (Eph) receptors and their ligands, ephrins, are expressed in many tissues and organs, and serve as a cell–cell communication system with a variety of roles in normal development, physiology and disease pathogenesis (Pasquale, 2005, 2010). These membrane proteins typically regulate cell adhesion and migration as well as cell–cell repulsion and adhesion by regulating the organisation of the actin cytoskeleton and modulating cell adhesion properties via integrins and other adhesion molecules. In mammals, Eph receptors are divided into classes EphA (A1–A8 and A10) and EphB (B1–B4 and B6) based on amino acid sequence homology of their extracellular domains (Pasquale, 2005, 2008). Members of these two receptor classes promiscuously bind to ligands of the ephrin-A (A1–A5) and -B (B1–B3) classes, respectively. This interaction of Eph receptors with ephrins results in bidirectional signal propagation in both receptor- and ligand-expressing cells (Pasquale, 2008, 2010; Kania and Klein, 2016). The roles of Eph receptors and ephrins have been extensively characterised in developing tissues, particularly in the central nervous system and vascular system, where they regulate axon guidance, tissue border formation, cell migration, vasculogenesis and angiogenesis (Kullander and Klein, 2002; Pasquale, 2005; Klein, 2012). Recently, Eph receptors and ephrins have also been implicated in the physiology and homeostasis of normal adult tissues and organs (Pasquale, 2008; Miao and Wang, 2009). Eph/ephrin signalling has been implicated in epithelial tissue homeostasis via regulation of epithelial compartments, cell positioning, proliferation, migration, adhesion and/or differentiation in several epithelial tissues including the intestine, stomach, mammary gland and epidermis (Miao and Wang, 2009; Ishii et al., 2011; Ogawa et al., 2013; Perez White and Getsios, 2014). Specific Eph/ephrin signalling is also involved in glucose homeostasis via modulation of insulin secretion in response to glucose levels in pancreatic islets

(Konstantinova et al., 2007), as well as bone maintenance and remodelling via regulation of osteoclast and osteoblast differentiation (Zhao et al., 2006).

In primary genital organs, several reports have indicated the expression and localisation of Eph receptors and ephrins in ovaries (Adu-Gyamfi et al., 2021). Buensuceso and Deroo showed that ephrin-A5 and EphA5 are localised in granulosa cells of the mouse ovary and that follicle-stimulating hormone upregulates *EFNA5*, *EPHA3*, *EPHA5* and *EPHA8* mRNA expression in mouse primary granulosa cells and a rat granulosa cell line (Buensuceso and Deroo, 2013). Ephrin-A5 has also been shown to be involved in folliculogenesis and ovulation, likely by mediating apoptosis, proliferation and steroidogenesis in the mouse (Buensuceso et al., 2016; Worku et al., 2018). Egawa et al. showed that ephrin-B1 is localised in theca interna cells and luteinising granulosa cells in the corpora lutea in the early luteal phase in human ovaries (Egawa et al., 2003). Moreover, certain Eph receptors and ephrins have been implicated in the progression and metastasis of ovarian carcinomas due to their upregulation or downregulation in these tumours (Adu-Gyamfi et al., 2021). On the other hand, in the testis, Gofur et al. recently showed that ephrin-B1 and EphB2/EphB4 exhibit complementary expression patterns in the epithelia along the excurrent duct system in the adult mouse testis and epididymis, and that these predominantly ephrin-B1- and EphB2/EphB4-expressing compartments are formed by two weeks of age in the mouse testis (Gofur and Ogawa, 2019; Gofur et al., 2020). They also showed that foetal Leydig cells weakly expressed ephrin-B1 and EphB4 in the mouse testis, while adult Leydig cells strongly expressed ephrin-B1. As both the adult and foetal Leydig cells commonly co-express ephrin-B1 and EphB4, the author hypothesised that ephrin-B1 and EphB4 are co-expressed ubiquitously in steroidogenic cells in gonads and other steroidogenic organs. To the best of the author's knowledge, however, the expression patterns and localisation of EphB receptors and ephrin-B ligands have not been sufficiently characterised in normal adult ovaries. In order

to test this hypothesis, therefore, the author examined ephrin-B1 and EphB4 expression and localisation initially in the naturally cycling mouse ovary, especially focusing on expression in steroidogenic cells, i.e. granulosa cells, steroidogenic theca cells, luteal cells and interstitial gland cells. Accordingly, the author found out that all types of steroidogenic cells co-expressed ephrin-B1 and EphB4 in the ovary. Therefore, the author believed that the hypothesis could be likely established.

The adrenal gland is a representative steroidogenic organ in addition to the testis and ovary (Miller and Auchus, 2011). The adrenal gland parenchyma consists of the medulla and cortex and is covered by a fibrous capsule in which stem/progenitor cells for the cortical steroidogenic cells reside (Simon and Hammer, 2012). The progenitor cells located in the periphery of the cortex migrate centripetally and repopulate the inner cortical zones upon differentiation (Belloni et al., 1978; Spencer et al., 1999). The adrenal cortex is composed of three zones as zona glomerulosa (zG) of the outer layer, zona fasciculata (zF) of the middle layer, and zona reticularis (zR) of the inner layer in many mammals while the cortex of aged mice is composed of zG and zF (Pihlajoki et al., 2015). The adrenal cortex of young mice contains an ephemeral layer between the zF and medulla known as the x-zone (xZ) (Hirokawa and Ishikawa, 1974; Morohashi and Zubair, 2011) which develops after birth and regresses in the male at puberty and in the female during the first pregnancy (Holmes and Dickson, 1971; Kim and Choi, 2020). Cells in the xZ are derived from the foetal adrenal gland and are involved in progesterone catabolism (Zubair et al., 2006; Hershkovitz et al., 2007).

A few reports have indicated expressions, localisations and/or functions of ephrins and Eph receptors in the adrenal glands (Adu-Gyamfi et al., 2021). Wang and his colleagues showed that chromaffin cells in the medulla of the adrenal glands expressed ephrin-B1 and EphB6 and the ephrin-B1/EphB6 signals were involved in catecholamine synthesis and secretion in concert with the nongenomic effect of testosterone in the male mouse (Wang et

al., 2018; Shi et al., 2019). Moreover, Brennan et al. showed that mRNAs of several ephrins and Eph receptors including ephrin-B1 and EphB4 mRNA expressed in the rat adrenal gland, and EphA2 and EphA3 protein were localised in zG (Brennan et al., 2008). To the best of the author's knowledge, however, the expression patterns and localisation of ephrin-B ligands and EphB receptors have not been sufficiently characterised in the adrenal glands. Thus, to test the author's hypothesis, expression and localisation of ephrin-B1 and EphB4 were examined in the adrenal gland especially focusing on steroidogenic cells in the adrenal cortex of the male and female mice.

Chapter 1

Identification of developmental/regressing stages of corpora lutea in the naturally cycling mouse ovary

Introduction

Corpora lutea appear in all oestrous phases of rodent ovaries undergoing the normal oestrous cycle up to 2 or 3 generations and are classified into three types as per their maturation status (Sato et al., 2016; Gaytan et al., 2017). The corpora lutea of the new generation (in the current oestrous cycle) appear as developing corpora lutea in the oestrus and metoestrus phases and as temporally mature corpora lutea primarily in the dioestrus and proestrus phases. The corpora lutea of the one- and two-cycle-old generation (in the previous cycles) appear as regressing corpora lutea in all four oestrous phases. In the preliminary experiments, the author found that ephrin-B1 immunoreactivity in luteal cells was largely similar within single corpus luteum in most corpora lutea, but rather different between corpora lutea in an ovary section, in which strongly and weakly ephrin-B1-expressing corpora lutea were mixed. It is difficult to precisely identify developmental/maturation/ regressing stages of corpora lutea by histological appearance in haematoxylin-eosin staining sections of the rodent ovaries even in which oestrous phases were determined by vaginal smear/cytology. Thus, the author sought to identify the developmental/maturation/regressing status of corpora lutea by a double immunofluorescence staining using anti-3β-HSD and CD31 antibodies with respect to 3β-HSD immunoreactivity in luteal cells and CD31-positive blood vessel densities. The author also examined the status of corpora lutea using a double immunofluorescence staining using anti-3β-HSD and F4/80 antibodies with respect to 3β-HSD immunoreactivity in luteal cells and F4/80-positive macrophage densities.

Materials and Methods

Animals

ICR female mice (8–9 weeks old) kept under standard housing (12 h light/12 h dark cycle; 22–23° C with 50–55 % humidity) and feeding conditions were used for immunohistochemical experiments. A total of 16 mice were used in this study. The phases of the oestrous cycle were determined according to the conventional vaginal smear/cytology (Cohen et al., 1997): vaginal smears were obtained daily, stained with Giemsa solution (Giemsa Stain Solution, FUJIFILM Wako Pure Chemical Corp., Osaka, Japan), and examined for cellular content; mice were assessed as being in one of the four phases of the cycle: oestrus, ~100 % cornified epithelial cells; metoestrus, ~50 % cornified epithelial cells and ~50 % leukocytes; dioestrus, 80–100 % leukocytes; or proestrus, ~100 % intact and live epithelial cells. After the assessment, mice were sacrificed by cervical dislocation or an overdose of pentobarbital (Nacalai Tesque, Kyoto, Japan), and the left ovaries were collected. Animal experimentation protocols were approved by the Animal Research Committee of Osaka Prefecture University (approval number: 30-16, 19-49, 20-32).

Antibodies

A rabbit polyclonal antibody against 3β-HSD, as a marker of steroidogenic cells in the ovary such as luteal cells, interstitial gland cells, and steroidogenic theca cells (Groten et al., 2006; Miyabayashi et al., 2015), was purchased from Trans Genic Inc. (KO607; Kobe, Japan). A rat monoclonal antibody against mouse CD31, as a marker of vascular endothelial cells (Gofur and Ogawa, 2019), was obtained from BD Biosciences (553370; Franklin Lakes, NJ, USA). A rat monoclonal antibody against mouse F4/80, as a marker of macrophages (Schaller et al., 2002), was obtained from BMA biomedicals (Rheinstrasse 28-32, CH-4302 Augst, Switzerland). Alexa Fluor 488-conjugated donkey anti-rabbit IgG (A-21206), Alexa Fluor

594-conjugated donkey anti-rabbit IgG (A-21207), and Alexa Fluor 594-conjugated donkey anti-rat IgG (A-21209) were obtained from Molecular Probes, Inc. (Eugene, OR, USA).

Immunofluorescence staining

The left ovaries in the four oestrous cycle phases were fixed with 10 % formalin in phosphate-buffered saline (PBS) for 4 h at 4°C. After washing with PBS, the tissues were immersed in 30 % sucrose in PBS overnight and mounted in optimum cutting temperature compound (Sakura Fine Technical Co., Ltd., Tokyo, Japan). Then, 6 μm-thick cryostat sections were cut and used for immunofluorescence staining. Single or double immunofluorescence staining was performed as previously described (Ogawa et al., 2011). Briefly, cryostat sections were incubated in a humid chamber with 1 % bovine serum albumin (BSA; A3059, Sigma-Aldrich, St Louis, MO, USA) in PBS (BSA-PBS), followed by incubation with single or mixed primary antibodies at a concentration of 1 μg/mL anti-3βHSD, 1:2,000 anti-CD31, and 1.5 μg/mL anti-F4/80 for 1.5 h at 32°C. After washing with PBS, the sections were incubated with (1) Alexa Fluor 488-conjugated donkey anti-rabbit IgG (5 μg/mL) in BSA-PBS, (2) a mixture of Alexa Fluor 488-conjugated donkey anti-rabbit IgG (5 μg/mL) and Alexa Fluor 594-conjugated donkey anti-rat IgG (5 μg/mL) for 30 min at 32°C. The sections were washed with PBS, mounted with PermaFluor (Thermo Fisher Scientific, Fremont, CA, USA), and photographed under an inverted fluorescence microscope (IX71; Olympus, Tokyo, Japan) using a digital camera (DP72; Olympus) controlled by the manufacturer's software (DP2-BSW; Olympus). Green fluorescence, red fluorescence, phase-contrast, and/or differential interference contrast images of the same field were captured using 4X, 10X, and 20X objective lenses (IX71, Olympus). Some of the immunostained sections were treated with an autofluorescence quenching reagent (TrueVIEW; Vector Laboratories, Inc., Burlingame, CA,

USA) according to the manufacture's protocol, with the following modification: mix reagents diluted 16 times by PBS were used instead of the original undiluted mix reagents.

Results

A 3β-HSD antibody has been used as a marker of steroidogenic cells such as luteal cells, interstitial gland cells, and steroidogenic theca cells in the ovary (Groten et al., 2006; Miyabayashi et al., 2015). CD31 has been used as a marker of vascular endothelial cells (Gofur and Ogawa, 2019). Thus developmental, maturing, and regressing features of corpora lutea were immunohistochemically identified by 3β-HSD immunoreactivity and CD31-positive blood vessel density in corpora lutea in naturally cycling mouse ovaries. The author used ovaries of the naturally cycling mice in which oestrous phases were clearly determined (Fig. 1-1). The 3β-HSD immunoreactivity in interstitial gland cells was prominent and similar among both interstitial glands and masses of cells from interstitial glands; it was also similar between the four oestrous cycle phases. Thus, the author defined the 3β-HSD immunoreactivity as similar to or somewhat lower than that observed in the interstitial glands as 'strong', and immunoreactivity less than that observed in interstitial glands as 'weak'. The 3β-HSD immunoreactivity was largely similar among luteal cells in many corpora lutea but appreciably different among corpora lutea in a section of the ovary (Fig. 1-2).

3β-HSD immunoreactivity was prominently different among luteal cells in certain corpora lutea, where strongly 3β-HSD-positive luteal cells were distributed sparsely in various degrees. Accordingly, corpora lutea could be roughly classified into three groups: corpora lutea occupied by largely weakly-3β-HSD-positive luteal cells, largely strongly-3β-HSD-positive luteal cells, and those consisting of a mixture of weakly- and strongly-3β-HSD-positive luteal cells in various ratios. By their CD31-positive blood vessel density, corpora lutea could be roughly classified into two groups: corpora lutea composed of blood vessels of

low and high density (Fig. 1-3). Moreover, CD31-positive thick blood vessels were sparsely distributed and ran towards the centre in some corpora lutea, while CD31-positive blood vessels were generally thin/fine in other corpora lutea. These characteristic corpora lutea frequently appeared in metoestrus and were filled with small 3β-HSD-positive cells. Based on these characteristic features, these corpora lutea could be identified as developing corpora lutea of the current oestrous cycle (CLd). The characteristic corpora lutea were composed of blood vessels of a prominently high density and strongly-3β-HSD-positive large luteal cells that frequently appeared in dioestrus and proestrus. These corpora lutea could be identified as temporally mature corpora lutea of the current oestrous cycle (CLm). Corpora lutea other than CLd and CLm, which composed of strongly 3β-HSD-positive luteal cells and CD31-positive blood vessels of low density as well as composed of weakly 3β-HSD-positive luteal cells and CD-31 positive blood vessels at a low or high density frequently appeared in all four phases and identified likely as regressing corpora lutea of the previous cycle and/or corpora lutea unable to undergo full differentiation into CLm (CLs). Moreover, the characteristic small corpora lutea were composed of strongly 3β-HSD-positive cells distributed sparsely and CD31-positive blood vessels of a prominently low density that frequently appeared in oestrus; based on these characteristic features, the author considered these corpora lutea as regressing corpora lutea of a late phase (CLrl).

After identification of developmental/maturation/regressing stages in corpora lutea by the combination of 3β-HSD immunoreactivity and CD31-positive vascular densities, the author examined macrophage densities in corpora lutea classified by the stages in naturally cycling mouse ovaries by 3β-HSD and F4/80 immunostaining. Based on F4/80-positive macrophage densities, corpora lutea could be largely classified into three groups: corpora lutea composed of F4/80-positive macrophage with low, medium, and high densities in the

naturally cycling mouse ovaries. By a combination of double immunostainings of 3β-HSD and F4/80 and the cycling phases, the three macrophage densities could correspond to stages of corpora lutea: corpora lutea appearing in low macrophage densities were CLd occupied with strongly-3β-HSD-positive small luteal cells as well as CLm occupied with strongly-3β-HSD-positive large luteal cells in the current cycle (Fig. 1-4). By contrast, corpora lutea appearing in medium macrophage densities were CLs, one or two-cycle old regressing/non-functional corpora lutea, occupied with largely strongly-3β-HSD-positive or weakly-3β-HSD-positive medium-sized luteal cells. Corpora lutea appearing in high macrophage densities were CLrl consisting of a mixture of weakly-and strongly-3β-HSD-positive luteal cells in the previous oestrous cycles (Fig. 1-5). Therefore, the combination of 3β-HSD-immunoreactivity and cell sizes of luteal cells as well as F4/80-positive macrophage densities might be also used for the identification of developmental/maturation/regressing stages of corpora lutea in naturally cycling mouse ovaries. The developmental stages of corpora lutea identified by combinations of 3β-HSD-immunoreactivity and cell sizes of luteal cells as well as vascular and macrophage densities are illustrated in Fig. 1-6.

Discussion

Corpora lutea appear in all oestrous phases of rodent ovaries undergoing the normal oestrous cycle up to 2 or 3 generations and are classified into three types as per their maturation status (Sato et al., 2016; Gaytan et al., 2017). It is difficult to precisely identify the maturation status of corpora lutea by histological appearance in haematoxylin-eosin staining sections of the rodent ovaries even in which oestrous phases were determined. Thus the author examined the maturation status of corpora lutea in the naturally cycling mouse ovaries using a combination of 3β-HSD immunoreactivity in luteal cells and CD31-positive blood vessel densities and identified characteristic corpora lutea comprising strongly- and weakly-3β-HSD-positive

small luteal cells and CD31-positive thick blood vessels at a low density running towards the centre. These corpora lutea were regarded as developing corpora lutea due to the number of small luteal cells and the characteristic vascular arrangement and their frequent appearance during metoestrus (Niswender et al., 2000; Fraser and Wulff, 2003; Gaytan et al., 2017), and termed CLd hereafter. The author identified other characteristic corpora lutea composed of strongly-3β-HSD-positive large cells and CD31-positive blood vessels at high density; these corpora lutea were regarded as temporally mature corpora lutea, due to the number of strongly-3β-HSD-positive large luteal cells, the high vascular density, and their frequent appearance during dioestrus and proestrus (Niswender et al., 2000; Fraser and Wulff, 2003; Gaytan et al., 2017), and termed CLm hereafter. Most other corpora lutea, such as those composed of (1) weakly-3β-HSD-positive luteal cells and blood vessels of a high or low density and (2) strongly-3β-HSD-positive luteal cells and blood vessels of low density, appeared in ovaries of all oestrous cycle phases. Thus the author regarded these as corpora lutea of an older generation in the previous oestrous cycle, i.e. regressing corpora lutea, or at least non-functional corpora lutea, due to the lack of the integrity in terms of the low 3β-HSD expression level and/or low vascular density, and termed these corpora lutea CLs. Moreover, the author also found corpora lutea composed of both strongly- and weakly-3β-HSD-positive luteal cells sparsely distributed to various degrees and thin blood vessels of very low densities; these corpora lutea were mostly small and appeared frequently in oestrus, and thus were almost certainly regressing corpora lutea of a late phase, due to the very low vascular densities and low luteal cell densities (Niswender et al., 2000; Fraser and Wulff, 2003; Gaytan et al., 2017), and termed CLrl. Previous reports showed that macrophages play a crucial role in luteolysis of corpora lutea in previous cycles via their cytokine production and phagocytic activity (Stein et al., 1992; Duncan et al., 1998). This was supported by the double

immunofluorescence staining using anti-3β-HSD and F4/80 antibodies: F4/80-positive macrophage densities were considerably high in CLrl.

Summary

Corpora lutea up to 2 or 3 generations appear in a section of rodent ovaries of all oestrous cycle phases (proestrus, oestrus, metoestrus, dioestrus). It is difficult to precisely identify the maturation status of corpora lutea by histological appearance in the rodent ovaries even in which oestrous phases were determined. By a double immunofluorescence staining using anti-3β-HSD and CD31 antibodies with respect to 3β-HSD immunoreactivity in luteal cells and CD31-positive blood vessel densities, maturation statuses of coprora lutea in the ovaries could be successfully identified, and accordingly coprora lutea were classified into four, i.e., CLd, CLm, CLs, and CLrl: CLd is developing corpora lutea comprising strongly- and weakly-3β-HSD-positive small luteal cells and CD31-positive thick blood vessels at a low density running towards the centre, and frequently present in metoestrus; CLm is temporally mature corpora lutea composed of strongly-3β-HSD-positive large cells and CD31-positive blood vessels at high density, and frequently present in dioestrus and proestrus; CLs is regressing/non-functional corpora lutea regarded as those of an older generation in the previous oestrous cycle, composed of (1) weakly-3β-HSD-positive luteal cells and blood vessels of a high or low density and (2) strongly-3β-HSD-positive luteal cells and blood vessels of low density, and present in all oestrous cycle phases; CLrl is regressing small corpora lutea of a late phase composed of both strongly- and weakly-3β-HSD-positive luteal cells sparsely distributed to various degrees and thin blood vessels of very low densities, and present frequently in oestrus. Because F4/80-positive macrophage densities were considerably high in CLrl, the double immunofluorescence staining using anti-3β-HSD and CD31 antibodies is likely applicable for the identification of CLrl.

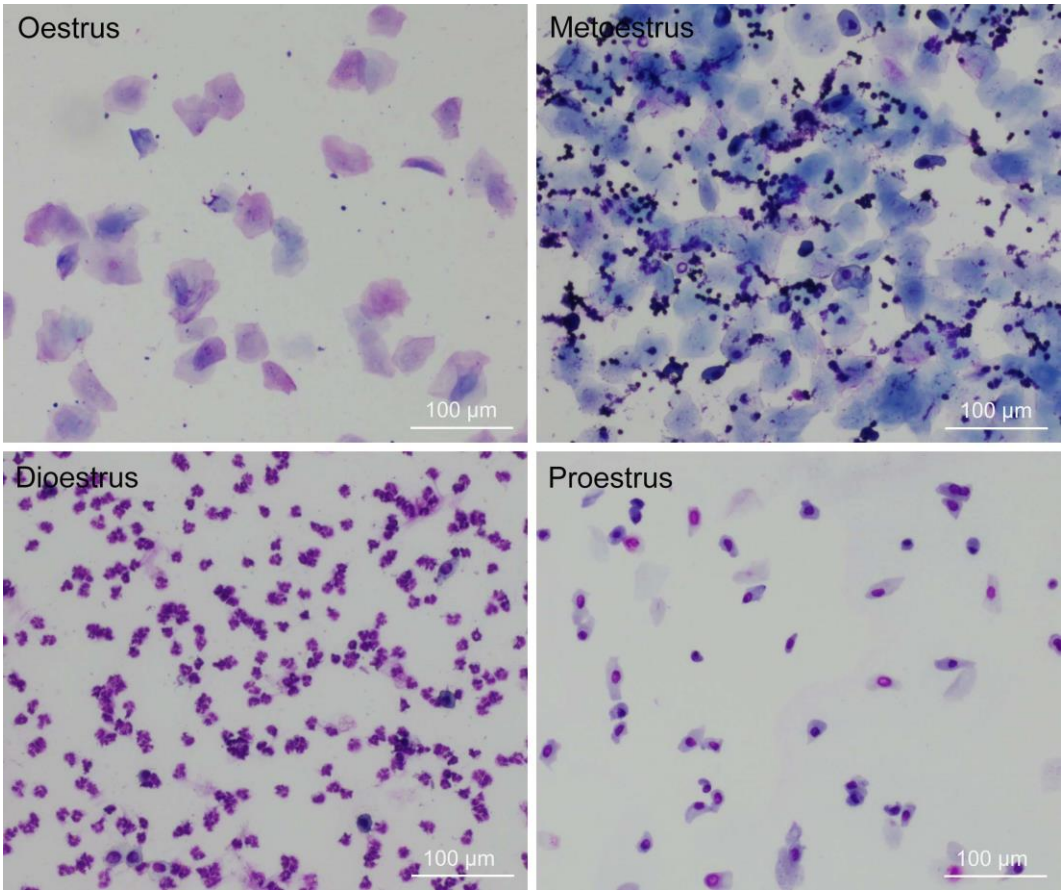
Oestrus
100 µm
Metoestrus
100 µm
Dioestrus
100 µm
Proestrus
100 µm

Fig. 1-1

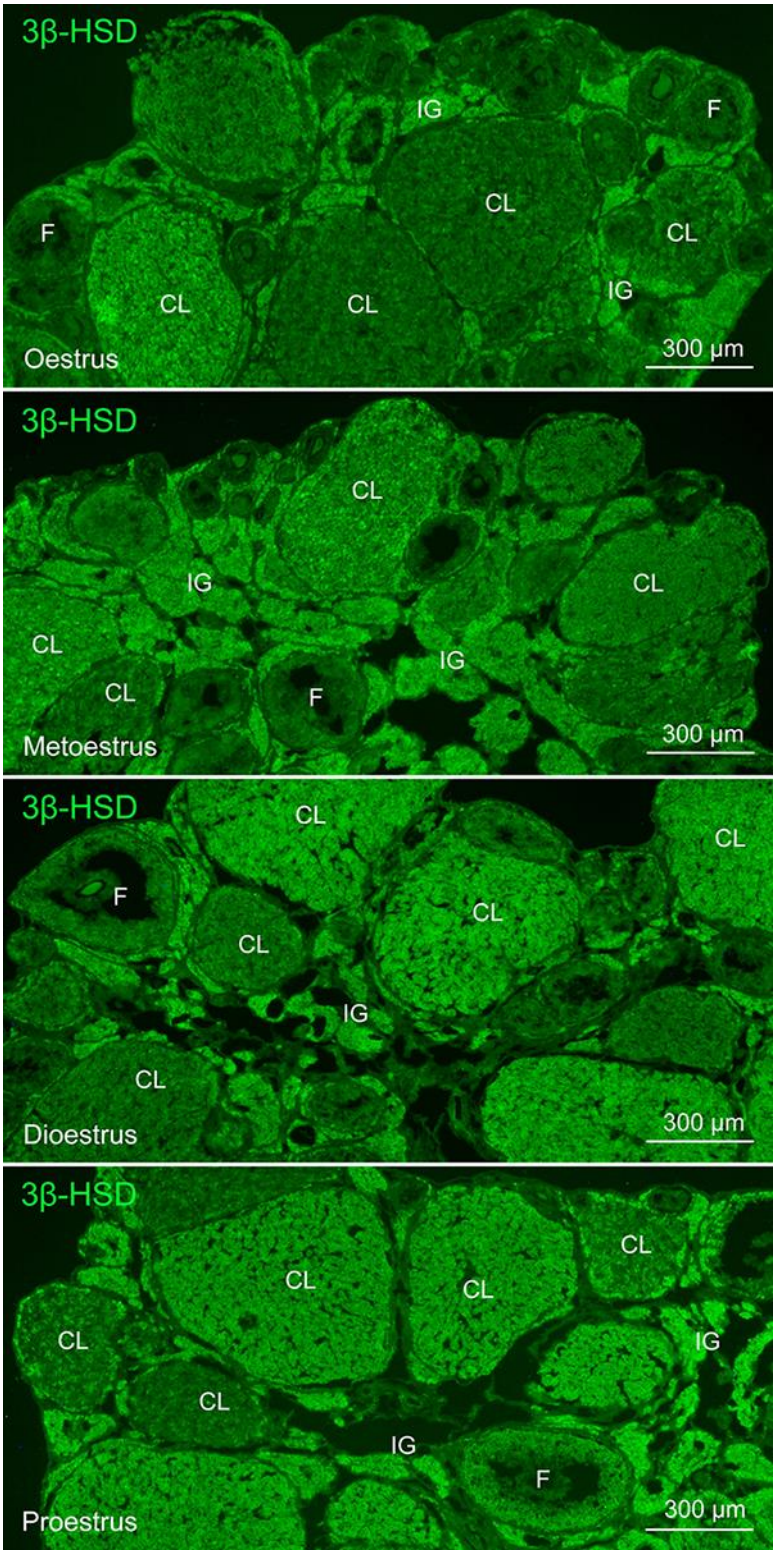
3β-HSD
IG
F
CL
F
CL
CL
CL
IG
Oestrus
300 µm
3β-HSD
CL
IG
CL
CL
IG
CL
F
Metoestrus
300 µm
3β-HSD
CL
CL
F
CL
CL
IG
CL
Dioestrus
300 µm
3β-HSD
CL
CL
CL
CL
IG
CL
IG
F
Proestrus
300 µm

Fig. 1-2

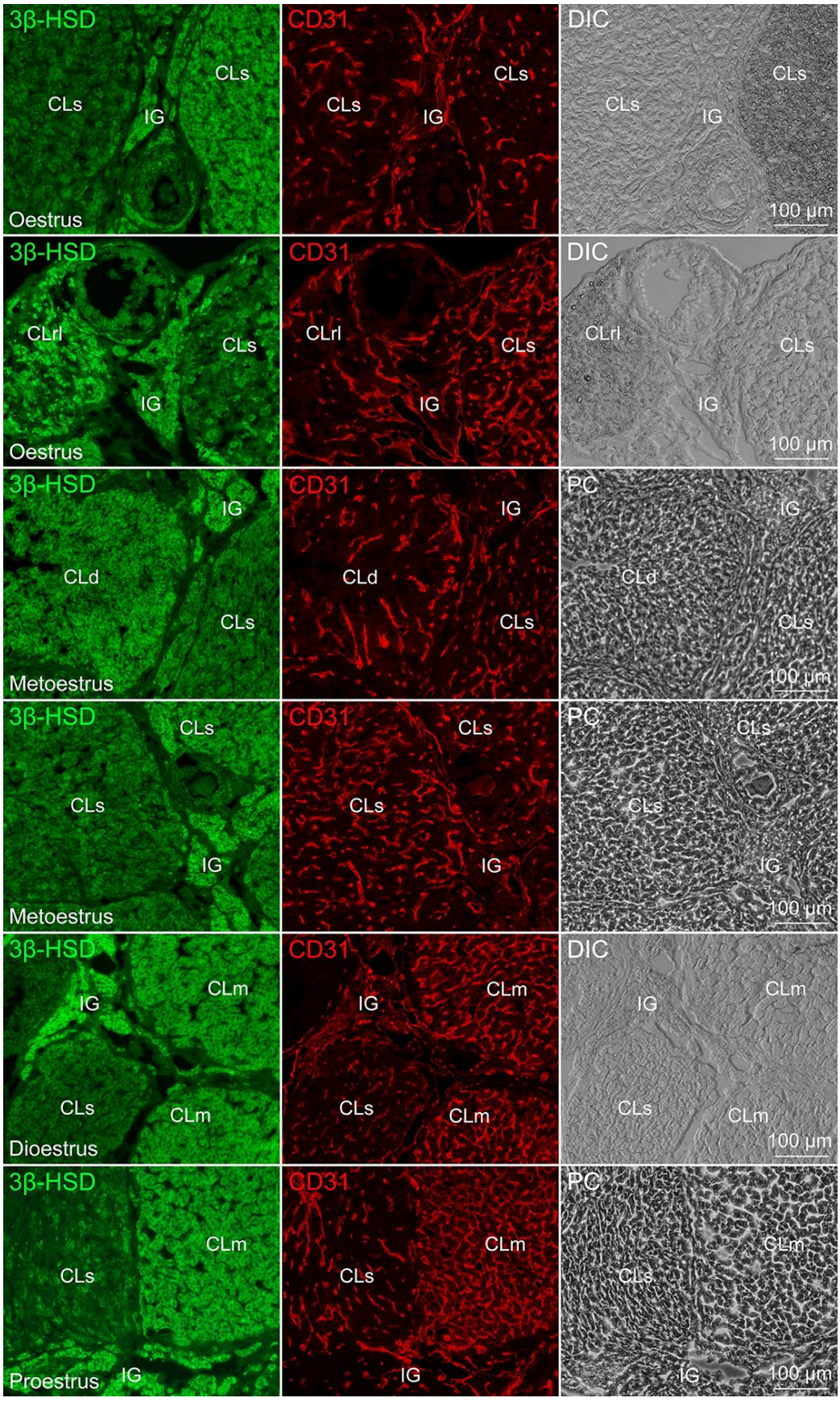
3β-HSD
CD31
DIC
CLs
IG
Oestrus
CLrl
Metoestrus
CLd
PC
CLm
Dioestrus
Proestrus
100 μm

Fig. 1-3

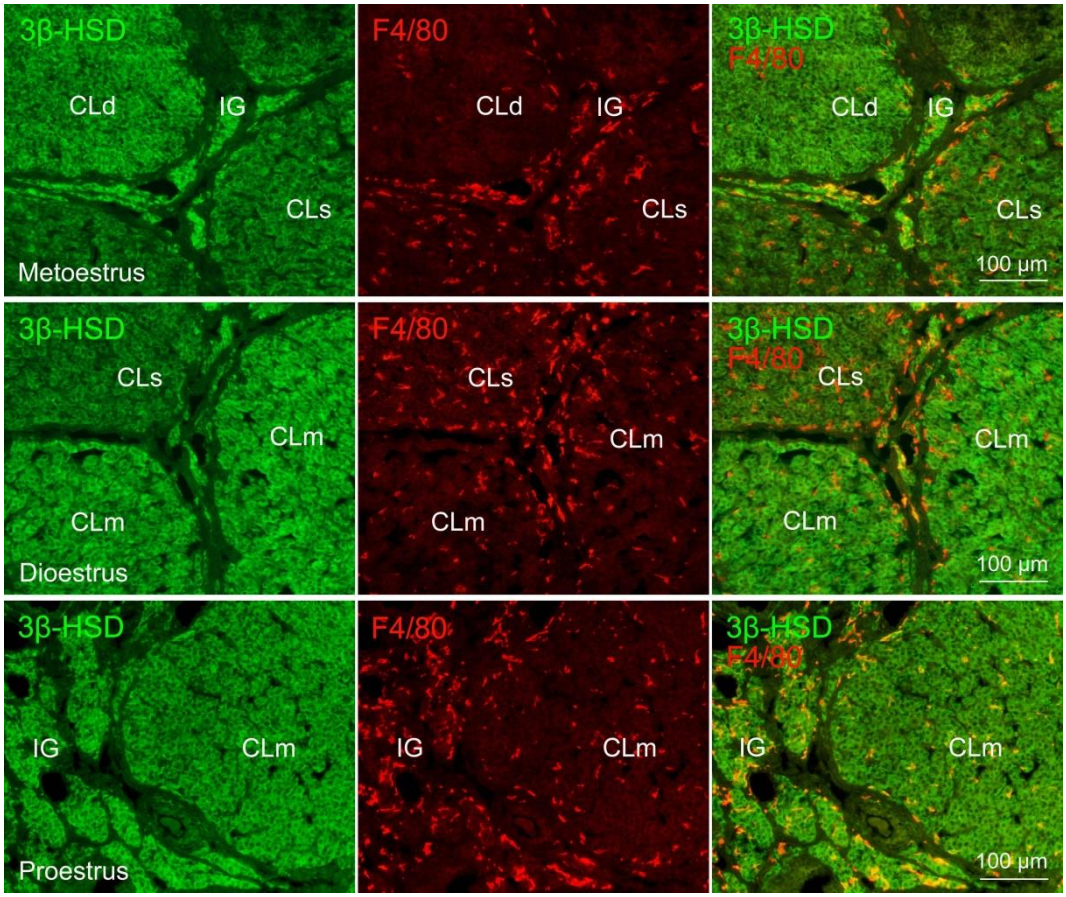
3β-HSD
CLd
IG
CLs
Metoestrus
F4/80
CLd
IG
CLs
3β-HSD
F4/80
CLd
IG
CLs
100 μm
3β-HSD
CLs
CLm
CLm
Dioestrus
F4/80
CLs
CLm
CLm
3β-HSD
F4/80
CLs
CLm
CLm
100 μm
3β-HSD
IG
CLm
Proestrus
F4/80
IG
CLm
3β-HSD
F4/80
IG
CLm
100 μm

Fig. 1-4

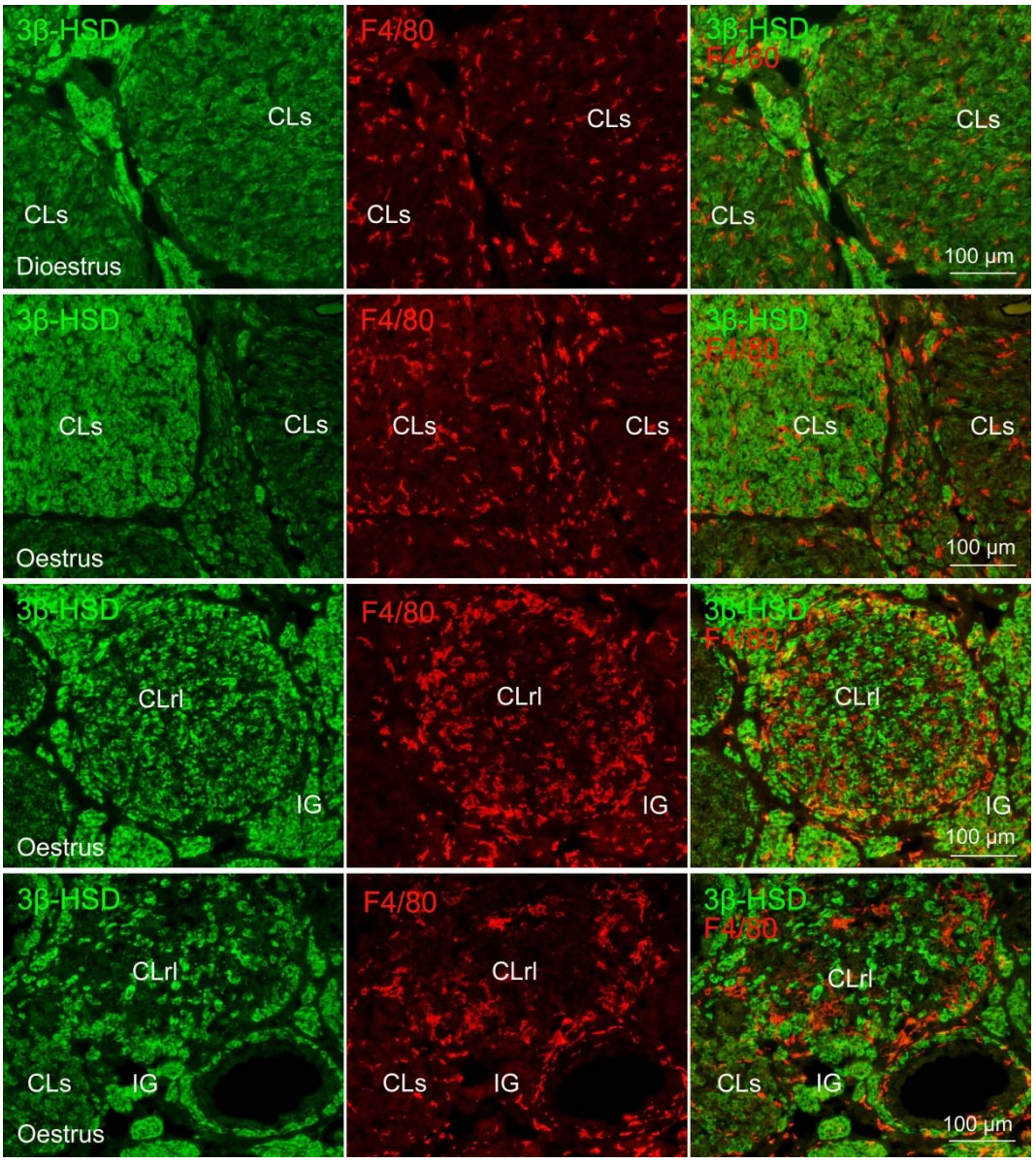
3β-HSD
CLs
CLs
Dioestrus
F4/80
CLs
CLs
3β-HSD
F4/80
CLs
CLs
100 μm
3β-HSD
CLs
CLs
Oestrus
F4/80
CLs
CLs
3β-HSD
F4/80
CLs
CLs
100 μm
3β-HSD
CLrl
IG
Oestrus
F4/80
CLrl
IG
3β-HSD
F4/80
CLrl
IG
100 μm
3β-HSD
CLrl
CLs
IG
Oestrus
F4/80
CLrl
CLs
IG
3β-HSD
F4/80
CLrl
CLs
IG
100 μm

Fig. 1-5

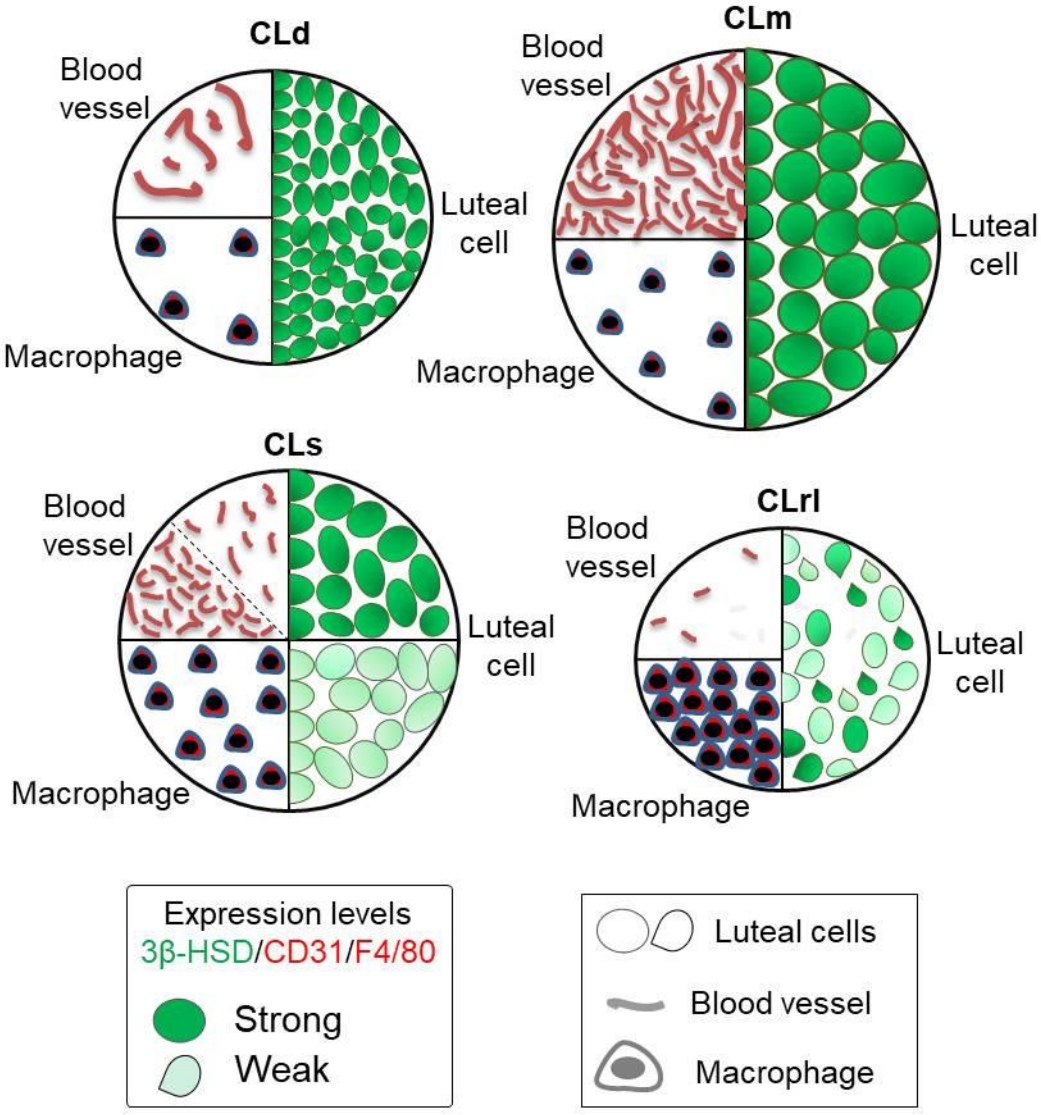
CLd
Blood vessel
Luteal cell
Macrophage
CLm
Blood vessel
Luteal cell
Macrophage
CLs
Blood vessel
Luteal cell
Macrophage
CLrl
Blood vessel
Luteal cell
Macrophage
Expression levels
3β-HSD/CD31/F4/80
Strong
Weak
Luteal cells
Blood vessel
Macrophage

Fig. 1-6

Figure legends

Figure 1-1

Representative Giemsa-staining vaginal smear images of four oestrous phases in naturally cycling mice. Three types of cells, i.e., leukocytes, large cornified epithelial cells, and nucleated small epithelial cells, appear at characteristic ratios in the respective oestrous phases (oestrus, metoestrus, dioestrus, proestrus).

Figure 1-2

Immunofluorescence micrographs showing overviews of 3β-HSD immunoreactivity in naturally cycling mouse ovaries at the four oestrous cycle phases. Note that 3β-HSD immunoreactivity is similar among interstitial glands but appreciably different among corpora lutea. CL, corpus luteum; F, follicle; IG, interstitial gland.

Figure 1-3

Double immunofluorescence micrographs showing features of 3β-HSD immunoreactivity in luteal cells and CD31-positive blood vessel density in corpora lutea of naturally cycling mouse ovaries. Sections were stained with the indicated antibodies, and green fluorescence (3β-HSD), red fluorescence (CD31), phase-contrast (PC), and/or differential interference-contrast (DIC) images of the same field were captured. Note that characteristic corpora lutea appear in specific phases: a small corpus luteum showing regressing features of a late phase is composed of strongly 3β-HSD-positive cells distributed sparsely and CD31-positive blood vessels of a prominently low density in the oestrus (CLrl); a corpus luteum showing developing features is fully occupied by 3β-HSD-positive small cells and CD31-positive thick blood vessels of a low density running towards the centre in the metoestrus (CLd); a corpus luteum showing temporally mature features is fully occupied by strongly-3β-HSD-positive

large cells and CD31-positive blood vessels of a prominently high density in the dioestrus and proestrus (CLm); a corpus luteum showing unfunctional features is composed of strongly 3β-HSD-positive luteal cells and CD31-positive blood vessels of low density as well as composed of weakly 3β-HSD-positive luteal cells and CD-31 positive blood vessels at a low or high density appeared in all four phases, and thus identified likely as regressing/non-functional corpora lutea of the previous cycle (CLs). CLs, corpus luteum of previous cycles (regressing/non-functional corpus luteum); CLd, developing corpus luteum; CLm, temporally mature corpus luteum; CLrl, regressing corpus luteum; IG, interstitial gland.

Figure 1-4

Double immunofluorescence micrographs showing features of 3β-HSD immunoreactivity of luteal cells and F4/80-positive macrophage density in corpora lutea of naturally cycling mouse ovaries. Sections were stained with the indicated antibodies, and green fluorescence (3β-HSD) and red fluorescence (F4/80) images of the same field were captured. Note that F4/80-positive macrophage densities are quite low in a corpus luteum showing developing features fully occupied by 3β-HSD-positive small cells (CLd). F4/80-positive macrophage densities are low in corpora lutea showing temporally mature features fully occupied by strongly-3β-HSD-positive large luteal cells (CLm). F4/80-positive macrophage densities are slightly high in corpora lutea showing regressing/non-functional features occupied by weakly-3β-HSD-positive luteal cells (CLs). CLs, corpus luteum of previous cycles; CLd, developing corpus luteum; CLm, temporally mature corpus luteum; IG, interstitial gland.

Figure 1-5

Double immunofluorescence micrographs showing features of 3β-HSD immunoreactivity of luteal cells and F4/80-positive macrophage densities in corpora lutea of naturally cycling

mouse ovaries. Sections were stained with the indicated antibodies, and green fluorescence (3β-HSD) and red fluorescence (F4/80) images of the same field were captured. F4/80-positive macrophage densities are slightly high in corpora lutea showing regressing/non-functional features occupied by weakly-3β-HSD-positive luteal cells or both strongly- and weakly-3β-HSD-positive luteal cells (CLs), and high in corpora lutea composed of strongly-3β-HSD-positive luteal cells sparsely distributed showing regressing features of a late phase (CLrl); CLs, corpus luteum of previous cycles; CLrl, regressing corpus luteum; IG, interstitial gland

Figure 1-6

Schematic drawings illustrating developmental/regressing stages of corpora lutea identified by combinations of 3β-HSD-immunoreactivity and cell sizes of luteal cells as well as vascular and macrophage densities in corpora lutea. CLd, a developing corpus luteum occupied by strongly-3β-HSD-positive small luteal cells, and composed of CD31-positive thick blood vessels running towards the centre and F4/80-positive macrophage at a low density; CLm, a temporally mature corpus luteum occupied by strongly-3β-HSD-positive large luteal cells and CD31-positive blood vessels at a prominently high density, and composed of F4/80-positive macrophages at a low density; CLs, a corpus luteum of the previous cycles composed of strongly 3β-HSD-positive luteal cells at a high density, CD31-positive blood vessels at a low density, and F4/80-positive macrophage at a medium-density as well as composed of weakly 3β-HSD-positive luteal cells at a high density, CD31-positive blood vessels at a low or high density, and F4/80-positive macrophage at a medium density; CLrl, a regressing corpus luteum of a late phase composed of strongly and/or weakly 3β-HSD-positive luteal cells distributed sparsely, CD31-positive blood vessels at a prominently low density, and F4/80-positive macrophage at a high density.

Chapter 2

Expression and localisation of ephrin-B1 and EphB4 in the naturally cycling mouse ovary

Introduction

Eph receptors and ephrins are expressed in many tissues and organs and serve as a cell-cell communication system with a variety of roles in normal development, physiology, and disease pathogenesis (Pasquale, 2005, 2010). In mammals, Eph receptors are divided into classes EphA (A1–A8 and A10) and EphB (B1–B4 and B6) based on amino acid sequence homology of their extracellular domains (Pasquale, 2005, 2008). Members of these two receptor classes promiscuously bind to ligands of the ephrin-A (A1–A5) and -B (B1–B3) classes, respectively. Recently, Eph receptors and ephrins have been implicated in the physiology and homeostasis of normal adult tissues and organs (Pasquale, 2008; Miao and Wang, 2009).

In primary genital organs, several reports have indicated the expression and localisation of Eph receptors and ephrins in ovaries (Adu-Gyamfi et al., 2021). Buensuceso and Deroo showed that ephrin-A5 and EphA5 are localised in granulosa cells of the mouse ovary and that follicle-stimulating hormone upregulates EFNA5, EPHA3, EPHA5, and EPHA8 mRNA expression in mouse primary granulosa cells and a rat granulosa cell line (Buensuceso and Deroo, 2013). Ephrin-A5 has also been shown to be involved in folliculogenesis and ovulation, likely by mediating apoptosis, proliferation, and steroidogenesis in the mouse (Egawa et al., 2003; Buensuceso et al., 2016). Egawa et al. showed that ephrin-B1 is localised in theca interna cells and luteinising granulosa cells in the corpora lutea in the early luteal phase in human ovaries (Egawa et al., 2003). On the other hand, in the testis, recently Gofur et al. showed that both foetal and adult Leydig cells commonly co-expressed ephrin-B1 and EphB4 in the mouse testis (Gofur and Ogawa, 2019; Gofur et al., 2020). Based on this, the author hypothesised that ephrin-B1 and EphB4 are co-

expressed ubiquitously in sex steroid-producing cells in gonads. To the best of the author's knowledge, however, the expression patterns and localisation of EphB receptors and ephrin-B ligands have not been sufficiently characterised in normal adult ovaries. In order to test this hypothesis, therefore, the author examined ephrin-B1 and EphB4 expression and localisation initially in the naturally cycling mouse ovary, focusing on expression in steroidogenic cells, i.e. granulosa cells, steroidogenic theca cells, luteal cells and interstitial gland cells. The author focused on ephrin-B1 and EphB4 expression patterns especially in luteal cells because luteal cells in different maturation/regression statuses appear in naturally cycling mouse ovaries.

Materials and Methods

Animals

ICR female mice (8-9 weeks old) kept under standard housing (12 h light/12 h dark cycle; 22-23 ^{o} C with 50-55 % humidity) and feeding conditions were used for reverse transcription-polymerase chain reaction (RT-PCR) and immunofluorescence staining experiments. A total of 28 mice were used in this study. The phases of the oestrous cycle were determined according to the conventional vaginal smear/cytology (Cohen et al., 1997) which is briefly described in Chapter 1. Animal experimentation protocols were approved by the Animal Research Committee of Osaka Prefecture University (approval number: 30-16, 19-49, 20-32).

Total RNA extraction and semi-quantitative RT-PCR analysis

Total RNA was isolated from the right ovary during each of the four oestrous cycle phases of naturally cycling ICR mice (oestrus, metoestrus, dioestrus, and proestrus) using TRizol reagent (Invitrogen, Carlsbad, CA, USA), and RT-PCR analysis was performed as previously described (Gofur and Ogawa, 2019). In brief, 1 µg total RNA was transcribed into first-strand

cDNA using M-MLV reverse transcriptase, RNase H- (Promega, Madison, WI, USA) and an oligo $(dT)_{18}$ primer, according to the manufacturer's instructions. For the detection of endogenous *EFNB1*, *EPHB4*, and *GAPDH*, 0.5 μL of the 25-μL reaction mixture was amplified with Taq DNA polymerase (TaKaRa Ex Taq HS; TaKaRa Bio Inc., Otsu, Japan) using the reverse-transcribed cDNA as template. The primer pairs and thermal cycling conditions used for PCR amplification in this experiment are shown in Table 2-1. The PCR cycle number was determined based on the linear amplification range obtained with samples in metoestrus when the expression levels were relatively high but similar among the four phases. The RT reaction was omitted for negative controls. PCR products were separated on 1.5 % agarose gels and visualised by ethidium bromide staining. The expression levels of amplified *EFNB1* and *EPHB4* mRNAs were determined from four independent experiments, normalised to the levels of *GAPDH* mRNA as an internal control (amplified over 23 cycles), and compared with those of the ovaries of mice in metoestrus.

Antibodies

Goat polyclonal antibodies against the mouse ephrin-B1 extracellular domain (AF473) and the mouse EphB4 extracellular domain (AF446) were purchased from R&D Systems, Inc. (Minneapolis, MN, USA). A rabbit polyclonal antibody against CYP17A1, as a marker of steroidogenic theca cells (Kakuta et al., 2018; Walters et al., 2019) was purchased from Proteintech (14447-1-AP; Rosemont, IL, USA). A rabbit polyclonal antibody against 3β-HSD, as a marker of steroidogenic cells in the ovary such as luteal cells, interstitial gland cells, and steroidogenic theca cells (Groten et al., 2006; Miyabayashi et al., 2015) was purchased from Trans Genic Inc. (KO607; Kobe, Japan). A rat monoclonal antibody against mouse CD31, as a marker of vascular endothelial cells (Gofur and Ogawa, 2019) was obtained from BD Biosciences (553370; Franklin Lakes, NJ, USA). A rat monoclonal antibody against mouse

thymic stromal cell antigen (ER-TR7), as a marker of fibroblasts and fibroblast-like cells, was obtained from Novus Biologicals (NB100-64932; Littleton, CO, USA). A rabbit polyclonal antibody against alpha-smooth muscle actin (α-SMA), as a marker of smooth muscle cells, was purchased from Abcam (ab5694; Cambridge, UK) to determine the theca externa of follicles. Alexa Fluor 488-conjugated donkey anti-goat IgG (A-11055), Alexa Fluor 488-conjugated donkey anti-rabbit IgG (A-21206), Alexa Fluor 594-conjugated donkey anti-rabbit IgG (A-21207), and Alexa Fluor 594-conjugated donkey anti-rat IgG (A-21209) were obtained from Molecular Probes, Inc. (Eugene, OR, USA).

Immunofluorescence staining

The left ovaries in the four oestrous cycle phases were fixed with 10 % formalin in phosphate-buffered saline (PBS) for ~4 h at 4°C. After washing with PBS, the tissues were immersed in 30 % sucrose in PBS overnight and mounted in optimum cutting temperature compound (Sakura Fine Technical Co., Ltd., Tokyo, Japan). Then, 6 μm-thick cryostat sections were used for immunofluorescence staining.

Single or double immunofluorescence staining was performed as previously described (Ogawa et al., 2011). Briefly, cryostat sections were incubated in a humid chamber with 1% BSA in PBS (BSA-PBS), followed by incubation with single or mixed primary antibodies at a concentration 1 μg/mL (anti-ephrin-B1, anti-3βHSD, anti-ER-TR7), 4 μg/mL (anti-EphB4), 1.4 μg/mL (anti-CYP17A1), 1:2,000 (anti-CD31) and 1:400 (α-SMA) for 1.5 h at 32°C. After washing with PBS, the sections were incubated with (1) Alexa Fluor 488-conjugated donkey anti-goat IgG (5 μg/mL) in BSA-PBS, (2) a mixture of Alexa Fluor 488-conjugated donkey anti-goat IgG (5 μg/mL) and Alexa Fluor 594-conjugated donkey anti-rabbit IgG (5 μg/mL), (3) a mixture of Alexa Fluor 488-conjugated donkey anti-goat IgG (5 μg/mL) and Alexa Fluor 594-conjugated donkey anti-rat IgG (5 μg/mL), or (4) a mixture of Alexa Fluor 488-

conjugated donkey anti-rabbit IgG (5 μg/mL) and Alexa Fluor 594-conjugated donkey anti-rat IgG (5 μg/mL) for 30 min at 32°C. The sections were washed with PBS, mounted with PermaFluor (Thermo Fisher Scientific, Fremont, CA, USA), and photographed under an inverted fluorescence microscope (IX71; Olympus, Tokyo, Japan) using a digital camera (DP72; Olympus) controlled by the manufacturer's software (DP2-BSW; Olympus). Green and red fluorescence images of the same field were captured using 4X, 10X, and 20X objective lenses (IX71, Olympus), and fluorescence micrographs were merged using Adobe Photoshop (San Jose, CA, USA). The specificity of the staining was verified by incubation without primary or secondary antibodies. Some of the immunostained sections were treated with an autofluorescence quenching reagent (TrueVIEW; Vector Laboratories, Inc., Burlingame, CA, USA) according to the manufacture's protocol, with the following modification: mix reagents diluted 16 times by PBS were used instead of the original undiluted mix reagents.

Semi-quantitative analyses on ephrin-B1 and EphB4 immunofluorescence intensities in steroidogenic cells

Relative immunofluorescence intensities of ephrin-B1 and EphB4 were semi-quantitatively analysed in steroidogenic cells (steroidogenic theca cells; granulosa cells; luteal cells in the developing, temporally mature, regressing/non-functional, and regressing corpora lutea of a late phase; interstitial gland cells) as well as in vascular endothelial cells in the corpora lutea (endothelial cells of thick and thin blood vessels in the corpora lutea) by densitometry. As ephrin-B1 and EphB4 immunoreactivities were similar among theca folliculi (theca interna cells) and follicles (granulosa cells), respectively, as well as during the four oestrous cycle phases, ephrin-B1 immunoreactivity in steroidogenic theca cells and EphB4 immunoreactivity in granulosa cells were used as controls to compare their expression levels among the

steroidogenic cells and vascular endothelial cells. Single and double fluorescence micrographs (2070 × 1548 pixels; captured by a 20X objective lens) in which follicles appeared in were selected. The expression levels of ephrin-B1 and EphB4 were determined from >5 micrographs per target steroidogenic cells/vascular endothelial cells; the fluorescence intensities of >10 regions (30 × 30 pixels/region) in each micrograph were measured in target steroidogenic theca and granulosa cells for ephrin-B1 and EphB4, respectively, as controls using ImageJ image processing programme (National Institutes of Health, Bethesda, MD, USA). The relative intensities to the controls were calculated from the average intensities of each micrograph.

Statistical analysis

Statistical analyses were performed with Microsoft Excel and statistical software available online (http://statpages.info/anova1sm.html). Differences in *EFNB1* and *EPHB4* mRNA expression levels among the four oestrous cycle phases as well as the differences in the ephrin-B1 and EphB4 expression levels between the target cells were evaluated by one-way analysis of variance (ANOVA), followed by Tukey's HSD post-hoc analysis. P-values less than 0.05 were considered significant. All values represent means ± SD.

Results

mRNA expression of ephrin-B1 and EphB4 in the oestrous phases

To investigate the relative expression levels of ephrin-B1and EphB4 in the four oestrous phases (oestrus, metoestrus, dioestrus, and proestrus) of naturally cycling mouse ovaries, semi-quantitative RT-PCR was performed. The transcripts of *EFNB1* and *EPHB4* were detected in all oestrous phases in the ovaries (Fig. 2-1A). The relative expression levels of *EFNB1* and *EPHB4* were similar among the four phases in the mouse ovaries (Fig. 2-1B).

These findings indicate that ephrin-B1 and EphB4 expression levels do not change in the whole ovary according to the oestrous cycle.

Ephrin-B1 immunoreactivity

To determine the localisation of the ephrin-B1 ligand in the naturally cycling mouse ovaries, the author performed single-and double-immunofluorescence staining of tissue sections: 3β-HSD immunostaining was used to identify steroidogenic cells such as luteal cells, interstitial gland cells, and steroidogenic theca cells in the ovaries; CD31 immunostaining was used to identify vascular endothelial cells; CYP17A1 immunostaining was used to identify steroidogenic theca interna cells in follicles; ER-TR7 immunostaining was used to identify theca folliculi by labeling fibroblasts and fibroblast-like cells; α-SMA immunostaining was used to identify the theca externa by labeling smooth muscle cells in this experiments.

Ephrin-B1 immunoreactivity was detected prominently in corpora lutea and theca folliculi in the naturally cycling mouse ovary (Fig. 2-2). No specific immunoreactivity was observed in control sections that had not been treated with primary or secondary antibodies (Fig. 2-2B). Ephrin-B1 immunoreactivity was similar among theca folliculi, as well as during the four oestrous cycle phases. Thus, the author defined ephrin-B1 immunoreactivity similar to or greater than that observed in the theca folliculi as ‘strong’, and immunoreactivity less than that in theca folliculi as ‘weak’ or ‘faint’. In contrast, ephrin-B1 immunoreactivity was appreciably different among corpora lutea in a section of ovaries (Fig. 2-2, 2-3). Ephrin-B1 immunoreactivity was localised in 3β-HSD-positive luteal cells and CD31-positive vascular endothelial cells distributed in corpora lutea, as well as stromal tissues (Fig. 2-3). Ephrin-B1 immunoreactivity was generally uniform and similar among luteal cells in a given corpus luteum: weakly or strongly ephrin-B1-positive luteal cells generally occupied a single corpus luteum. By contrast, in certain small corpora lutea where 3β-HSD-positive luteal cells were

not fully occupied, 3β-HSD-positive luteal cells appeared to include both strongly and weakly ephrin-B1-positive cells (Fig. 2-3). As noted above, ephrin-B1 immunoreactivity varied widely among corpora lutea; therefore, ephrin-B1 immunoreactivity was thoroughly examined in corpora lutea by double immunofluorescence staining with ephrin-B1 and 3β-HSD, and with ephrin-B1 and CD31 in serial sections. The author found that ephrin-B1 immunoreactivity was weak in CLd: developing corpora lutea that were frequently present in metoestrus (Fig. 2-4). Moreover, ephrin-B1 immunoreactivity was also weak in CLm: temporally mature corpora lutea that were frequently present in dioestrus and proestrus (Fig. 2-4). By contrast, ephrin-B1 immunoreactivity was strong in CLs: one or two-cycle old regressing/non-functional corpora lutea (1) largely composed of weakly-3β-HSD-positive luteal cells and CD31-positive blood vessels of a high density, as well as (2) largely composed of strongly- or weakly-3β-HSD-positive luteal cells and CD31-positive blood vessels of a low density (Fig. 2-5). Moreover, ephrin-B1 immunoreactivity varied in the relatively small CLrl: regressing corpora lutea of a late phase that were frequently present in oestrus (Fig. 2-3, 2-5).

Ephrin-B1 immunoreactivity was also detected weakly in 3β-HSD-positive interstitial gland cells in the four oestrous cycle phases of naturally cycling mouse ovaries (Figs. 2-3–6). Ephrin-B1 immunoreactivity was faint but substantial in granulosa cells and oocytes in follicles (Fig. 2-6). Moreover, ephrin-B1 was expressed in theca folliculi, which were largely marked by ER-TR7 immunoreactivity. Ephrin-B1 immunoreactivity was strong in cells of the thick inner layer (theca interna) and weak/faint in cells of the thin outer layer (theca externa), which was composed of α-SMA-positive smooth muscle cells. Ephrin-B1 was expressed strongly in CYP17A1-positive steroidogenic theca cells, which were sparse in the inner layer, i.e. theca interna (Fig. 2-6). These qualitative expression levels of ephrin-B1 immunoreactivity (strong, weak, faint) nearly corresponded to those that were semi-quantitatively determined from cellular fluorescence intensities in the steroidogenic cells in

corpora lutea and follicles and normalised to/compared with those of the theca cells as controls (standard), via densitometric quantification using the ImageJ image processing programme (Fig. 2-7).

EphB4 immunoreactivity

To determine the localisation of the EphB4 receptors in the naturally cycling mouse ovary, the author performed single-and double-immunofluorescence staining of tissue sections: CD31 immunostaining was used to identify vascular endothelial cells; CYP17A1 immunostaining was used to identify steroidogenic theca interna cells in follicles; ER-TR7 immunostaining was used to identify theca folliculi by labeling fibroblasts and fibroblast-like cells; α-SMA immunostaining was used to identify the theca externa by labeling smooth muscle cells in this experiments.

EphB4 immunoreactivity was detected prominently in vasculature in the stroma and follicles (Fig. 2-8A). EphB4 immunoreactivity was similar among vasculatures in the stroma and among follicles, as well as among the four oestrous cycle phases in the naturally cycling mouse ovaries. EphB4 immunoreactivity was also detected in corpora lutea, where EphB4 immunoreactivity and expression patterns varied. No specific immunoreactivity was observed in control sections that had not been treated with primary or secondary antibodies (Fig. 2-8B). In developing corpora lutea (CLd), EphB4 immunoreactivity was relatively strong in CD31-positive vascular endothelial cells and weak in CD31-negative small round cells, i.e. luteal cells (Fig. 2-9A). In temporally mature corpora lutea (CLm), EphB4 expression varied in CD31-positive vascular endothelial cells; it was strong in thick/relatively large blood vessels and weak in thin blood vessels (Fig. 2-9A). In CLm, EphB4 immunoreactivity was also detected weakly in CD31-negative large round/polygonal cells, i.e. luteal cells. By contrast in CLs composed of CD31-positive thin blood vessels of a low density, EphB4

immunoreactivity was weakly detected in blood vessels but was not apparent in CD31-negative cells (Fig. 2-9A).

EphB4 immunoreactivity was prominent/strong in granulosa cells and weak in oocytes in follicles (Fig. 2-9B). Moreover, EphB4 was expressed in cells composed of theca folliculi: weakly/faintly in CYP17A1-positive steroidogenic cells, CD31- positive vascular endothelial cells, ER-TR7-positive fibroblastic cells, and α-SMA-positive smooth muscle cells (Fig. 2-9B). EphB4 immunoreactivity was also detected weakly in interstitial gland cells in the four oestrous phases of naturally cycling mouse ovaries (Fig. 2-9B). These qualitative expression levels of EphB4 immunoreactivity (strong, weak, faint) nearly corresponded to those that were semi-quantitatively determined from cellular fluorescence intensities in the steroidogenic cells in follicles and corpora lutea, and normalised to/compared with those of granulosa cells as controls (standard), via densitometric quantification using the image processing programme (Fig. 2-10). The present findings indicate that both ephrin-B1 and EphB4 are substantially co-expressed in all steroidogenic cells in the ovaries, i.e. luteal cells, granulosa cells, steroidogenic theca cells, and interstitial gland cells, while their expression levels vary especially in corpora lutea.

Discussion

Eph receptors and ephrins are membrane proteins that act as a cell–cell communication system. Recently, Gofur et al. found that not only adult Leydig cells but also foetal Leydig cells co-express ephrin-B1 and EphB4 in the mouse testes (Gofur and Ogawa, 2019; Gofur et al., 2020). Based on this finding, the author speculated that sex steroid-producing cells may commonly co-express ephrin-B1 and EphB4 and examined their expression in the naturally cycling mouse ovaries in this study. Accordingly, the author observed that ephrin-B1 and EphB4 are co-expressed in sex steroid-producing cells of several types present in the ovary,

i.e. granulosa cells, and in CYP17A1-positive steroidogenic theca cells as well as luteal cells and 3β-HSD-positive interstitial gland cells. A previous study partially supports the author's findings, as ephrin-B1 was found to be localised in the theca interna cells and luteinising granulosa cells in the corpora lutea of the early luteal phase in human ovaries (Egawa et al., 2003). To the best of the author's knowledge, there are no other studies investigating the localisation of ephrin-B1 and EphB4 in the ovaries, and thus, this is the first report clearly showing ephrin-B1 and EphB4 localisation in normal adult ovaries. It is now well accepted that sex steroid-producing cells reside in extra-gonadal organs/tissues such as brains and adipose tissues, and that steroids produced by these cells function as local mediators (Nikolakis et al., 2016; Larson, 2018; Rubinow, 2018). Thus, the author proposes that co-expression of ephrin-B1 and EphB4 may represent a good marker to identify sex steroid-producing cells even in extra-gonadal organs/tissues. Further investigation will be required to determine the common co-expression of ephrin-B1 and EphB4 in extra-gonadal organs/tissues. Moreover, the author found steroidogenic theca cells strongly express ephrin-B1 and weakly express EphB4. This expression pattern is quite similar to that in mouse adult Leydig cells (Gofur and Ogawa, 2019). Steroidogenic theca cells synthesise androgens in response to luteinising hormone (LH) stimuli (Young and McNeilly, 2010). The androgen synthesis in theca cells through LH stimuli is similar to that in Leydig cells (Zirkin and Papadopoulos, 2018). Thus, the expression pattern of ephrin-B1 and EphB4 may be a possible marker for androgen-producing cells. Again, further investigation is required to confirm this supposition.

The author found that ephrin-B1 and EphB4 immunoreactivity are similar among the same type of tissues/cells, excepting corpora lutea between the four oestrous cycle phases in naturally cycling mouse ovaries. Ephrin-B1 immunoreactivity in luteal cells was largely similar within single corpus luteum in most corpora lutea, but rather different between corpora lutea in an ovary section, in which strongly and weakly ephrin-B1-expressing corpora lutea

were mixed. Therefore in Chapter 1, the author examined the maturation status of corpora lutea using a combination of 3β-HSD immunoreactivity in luteal cells and CD31-positive blood vessel densities and identified maturation statuses of corpora lutea in the naturally cycling mouse ovaries, and accordingly, corpora lutea were classified into four, i.e., CLd (developing corpora lutea frequently present in metoestrus), CLm (temporally mature corpora lutea frequently present in dioestrus and proestrus), CLs (regressing/non-functional corpora lutea of an older generation in the previous oestrous cycle), and CLrl (regressing small corpora lutea of a late phase present frequently in oestrus). Ephrin-B1 expression in luteal cells was weak in CLd and CLm regarded as newly-formed corpora lutea in the current oestrous cycle. By contrast, ephrin-B1 expression in luteal cells was strong/prominent in most other corpora lutea, i.e., CLs showing the lack of the integrity in terms of the low 3β-HSD expression level and/or low vascular density. Moreover, the author also found that ephrin-B1 expression in luteal cells varied in CLrl.

Ephrin-B1 expression patterns in corpora lutea are largely summarised as follows according to the author's above identification of the development/maturation/regression phases of corpora lutea: ephrin-B1 expression in luteal cells is weak in developing and temporally mature corpora lutea of the current oestrous cycles and strong in regressing corpora lutea of the previous cycle. Similar to ephrin-B1 expression in luteal cells, EphB4 immunoreactivity in luteal cells was largely similar within a single corpus luteum: EphB4 expression in luteal cells was weak in newly-formed corpora lutea of the current oestrous cycle and faint/negative in regressing corpora lutea of the previous cycles. Moreover, the author found that ephrin-B1 and EphB4 expression in granulosa cells was faint and strong, respectively. Therefore, it could be likely summarised that the upregulation of ephrin-B1 expression in luteal cells occurs at the transformation of granulosa cells into luteal cells and thereafter additionally at the time of the generation transition in corpora lutea, i.e. regressing

corpora lutea, and that *vice versa* the downregulation of EphB4 expression in luteal cells occurs at both of these time points. These findings are partly supported by a previous study showing ephrin-B1 expression induction during the transformation of granulosa cells into luteal cells in human ovaries (Egawa et al., 2003). In naturally cycling rodents, the surge of hormones targeted to granulosa cells and/or luteal cells, such as LH and prolactin, occurs around those phases (Sato et al., 2016). The LH surge triggers the transformation of granulosa cells and steroidogenic theca cells into luteal cells and causes the regression of corpora lutea (luteolysis) (Stocco et al., 2007; Duffy et al., 2019); thus, these hormones may be candidate molecules to induce the upregulation of ephrin-B1 expression and downregulation of EphB4 in luteal cells. Further investigation is required to determine whether and how ephrin-B1 is upregulated and EphB4 is downregulated at these times.

Angiogenesis actively occurs during the luteinisation and development of corpora lutea triggered by the LH surge (Fraser and Wulff, 2003). The author found that EphB4 in CD31-positive vascular cells is strong in developing and temporally mature corpora lutea (CLd and CLm), while ephrin-B1 expression in the vascular cells is largely weak in most oestrous cycle phases. This finding is partly supported by a previous report, in which EphB4/ephrin-B1 signalling is implicated in angiogenesis (Adams et al., 1999). The overall ephrin-B1 and EphB4 expression patterns and levels in the steroidogenic cells of the mouse ovary are illustrated in Fig. 2-11. The relative expression levels in the illustration are supported by the semi-quantitative analyses: the expression levels of ephrin-B1 and EphB4 in the steroidogenic cells in the corpora lutea and follicles as well as in the vascular endothelial cells in the corpora lutea were semi-quantitatively determined from cellular fluorescence intensities and normalised to/compared with those of the theca cells and granulosa cells as controls (standard), respectively, via densitometric quantification using ImageJ image processing programme (Fig. 2-7, 2-10).

In conclusion, this study represents the first detailed expression/localisation analysis of ephrin-B1 and EphB4 in normal and naturally cycling mouse ovaries. The author found that ephrin-B1 and EphB4 are co-expressed in sex steroid-producing cells of all types present in the ovary. As Gofur et al. previously observed the co-expression of ephrin-B1 and EphB4 in adult and foetal Leydig cells (Gofur and Ogawa, 2019; Gofur et al., 2020), the author concluded that their co-expression is likely common in sex steroid-producing cells, and thus, possibly represents a good marker to identify sex steroid-producing cells even in extra-gonadal organs/tissues. The author also found that (1) ephrin-B1 and EphB4 expression in granulosa cells is faint and strong, respectively; that (2) ephrin-B1 expression in luteal cells is weak in developing and temporally mature corpora lutea (corpora lutea of the current oestrous cycle) and strong in regressing corpora lutea (corpora lutea of the previous cycles) and that (3) by contrast, EphB4 expression in luteal cells is weak in corpora lutea of the current oestrous cycle and faint/negative in corpora lutea of the previous cycles. The surge of pituitary hormones such as LH may trigger the upregulation of ephrin-B1 and downregulation of EphB4 expression, because their fluctuation begins immediately after the surge. Although further investigation is required to provide in-depth clarification of the role of these molecules in the ovaries, the expression patterns of the ephrin-B ligand and EphB receptor may represent benchmarks for examining steroidogenic cells in the ovaries.

Summary

This study represents the first detailed expression/localisation analysis of ephrin-B1 and EphB4 in normal and naturally cycling mouse ovaries. The author found that ephrin-B1 and EphB4 are co-expressed in sex steroid-producing cells of all types present in the ovary. Because Gofur et al. previously reported the co-expression of ephrin-B1 and EphB4 in adult and foetal Leydig cells, the author concluded that their co-expression is likely common in sex

steroid-producing cells, and thus, possibly represents a good marker to identify sex steroid-producing cells even in extra-gonadal organs/tissues. The author also found that (1) ephrin-B1 and EphB4 expression in granulosa cells is faint and strong, respectively; that (2) ephrin-B1 expression in luteal cells is weak in developing and temporally mature corpora lutea (corpora lutea of the current oestrous cycle) and strong in regressing corpora lutea (corpora lutea of the previous cycles) and that (3) by contrast, EphB4 expression in luteal cells is weak in corpora lutea of the current oestrous cycle and faint/negative in corpora lutea of the previous cycles. The surge of pituitary hormones such as LH may trigger the upregulation of ephrin-B1 and downregulation of EphB4 expression, because their fluctuation begins immediately after the surge. Although further investigation is required to provide in-depth clarification of the role of these molecules in the ovaries, the expression patterns of the ephrin-B ligand and EphB receptor may represent benchmarks for examining steroidogenic cells in the ovaries.

Table 2-1. Primers and cycle numbers for PCR amplification

Primer			Product size (bp)	Annealing temp. (°C)	Cycle number
ephrin-B1	Forward	5′-TGCTTGATCCCAATGTACTG-3′	520	55.0	29
	Reverse	5′-CGGAGCTTGAGTAGTAGGAC-3′			
EphB4	Forward	5′-AGCCCCAAATAGGAGACGAG-3′	540	57.9	34
	Reverse	5′-GGATAGCCCATGACAGGATC-3′			
GAPDH	Forward	5′-GACTCCACTCACGGCAAATT-3′	689	57.5	23
	Reverse	5′-TCCTCAGTGTAGCCCAAGAT-3′			

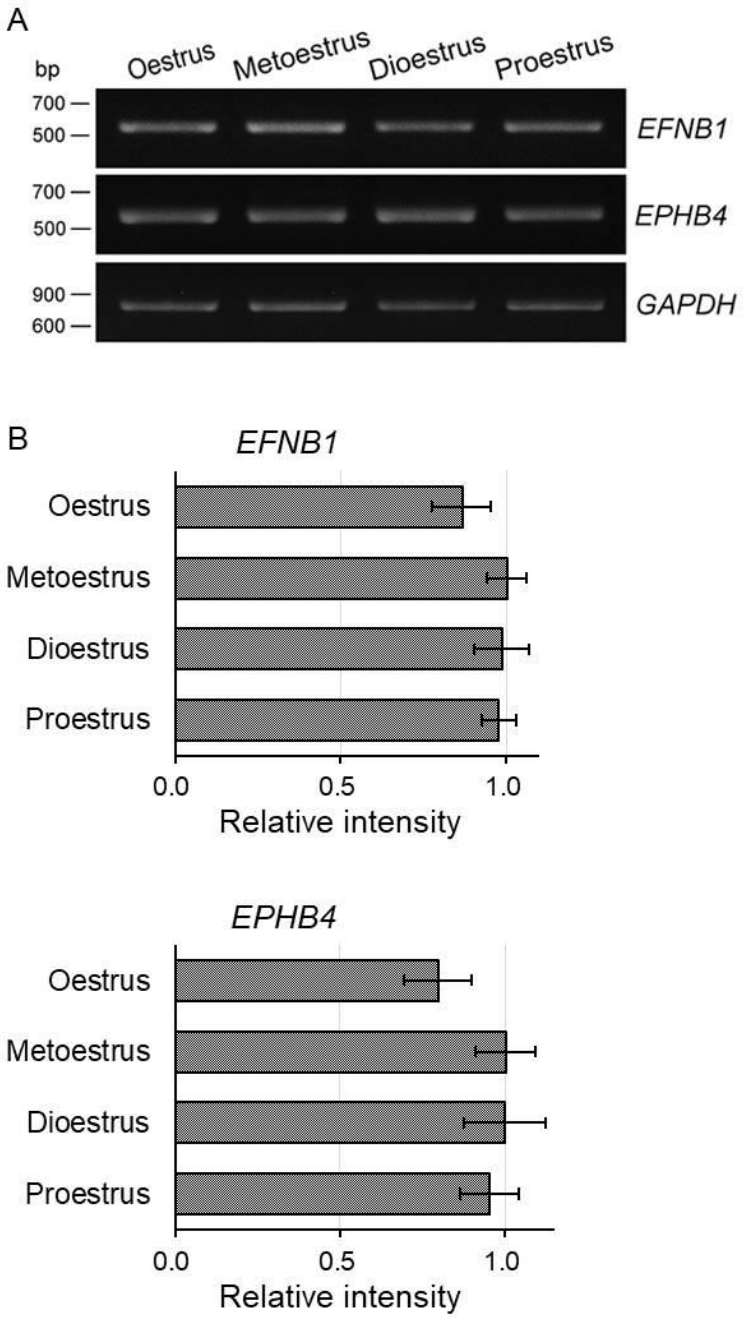
A
bp
Oestrus
Metoestrus
Dioestrus
Proestrus
700
500
EFNB1
700
500
EPHB4
900
600
GAPDH
B
EFNB1
Oestrus
Metoestrus
Dioestrus
Proestrus
0.0
0.5
1.0
Relative intensity
EPHB4
Oestrus
Metoestrus
Dioestrus
Proestrus
0.0
0.5
1.0
Relative intensity

Fig. 2-1

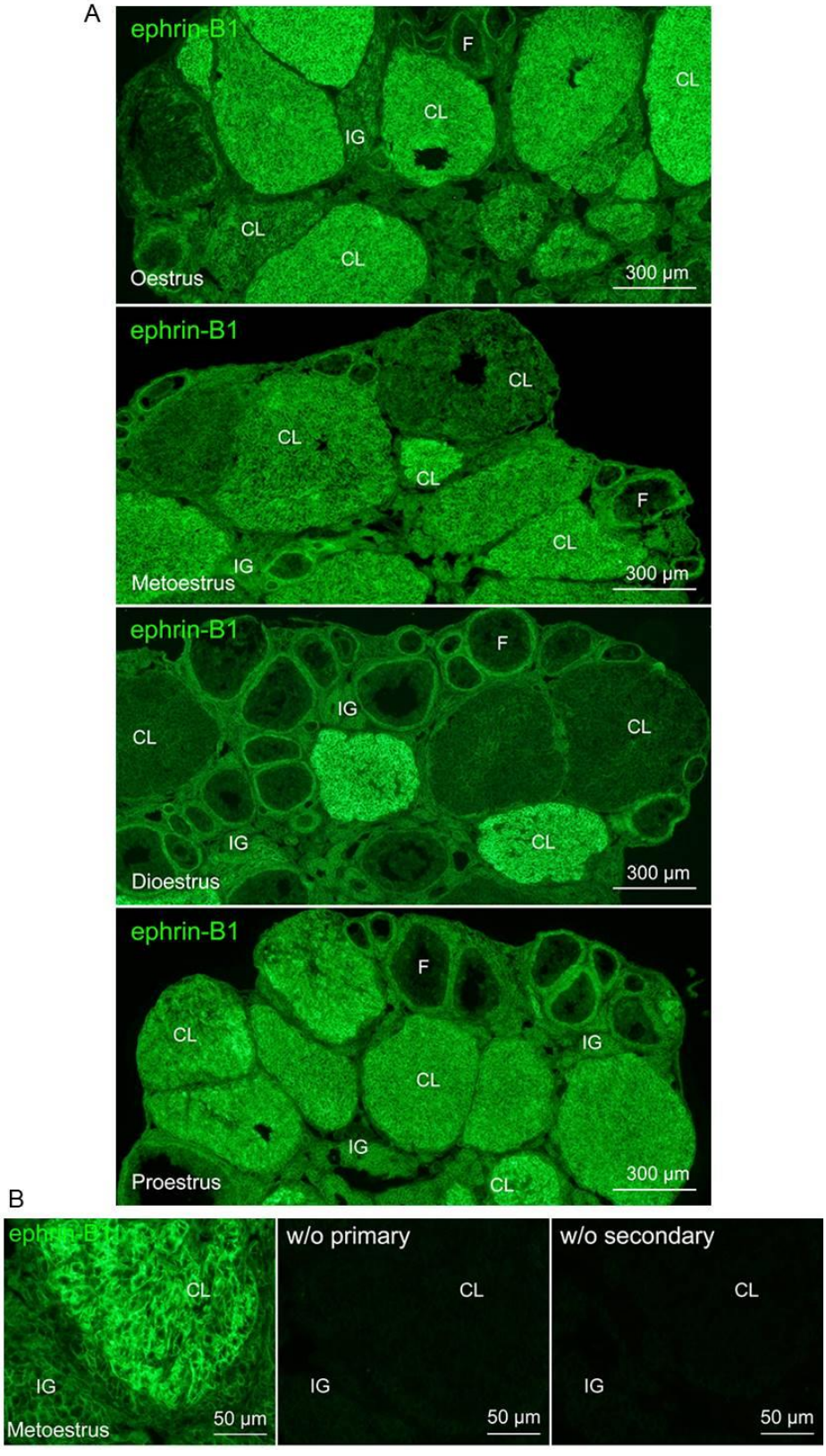
A
ephrin-B1
F
CL
IG
CL
CL
CL
Oestrus
300 µm
ephrin-B1
CL
CL
CL
F
CL
IG
Metoestrus
300 µm
ephrin-B1
F
IG
CL
CL
IG
CL
Dioestrus
300 µm
ephrin-B1
F
CL
IG
CL
IG
Proestrus
CL
300 µm
B
CL
IG
Metoestrus
50 µm
w/o primary
CL
IG
50 µm
w/o secondary
CL
IG
50 µm

Fig. 2-2

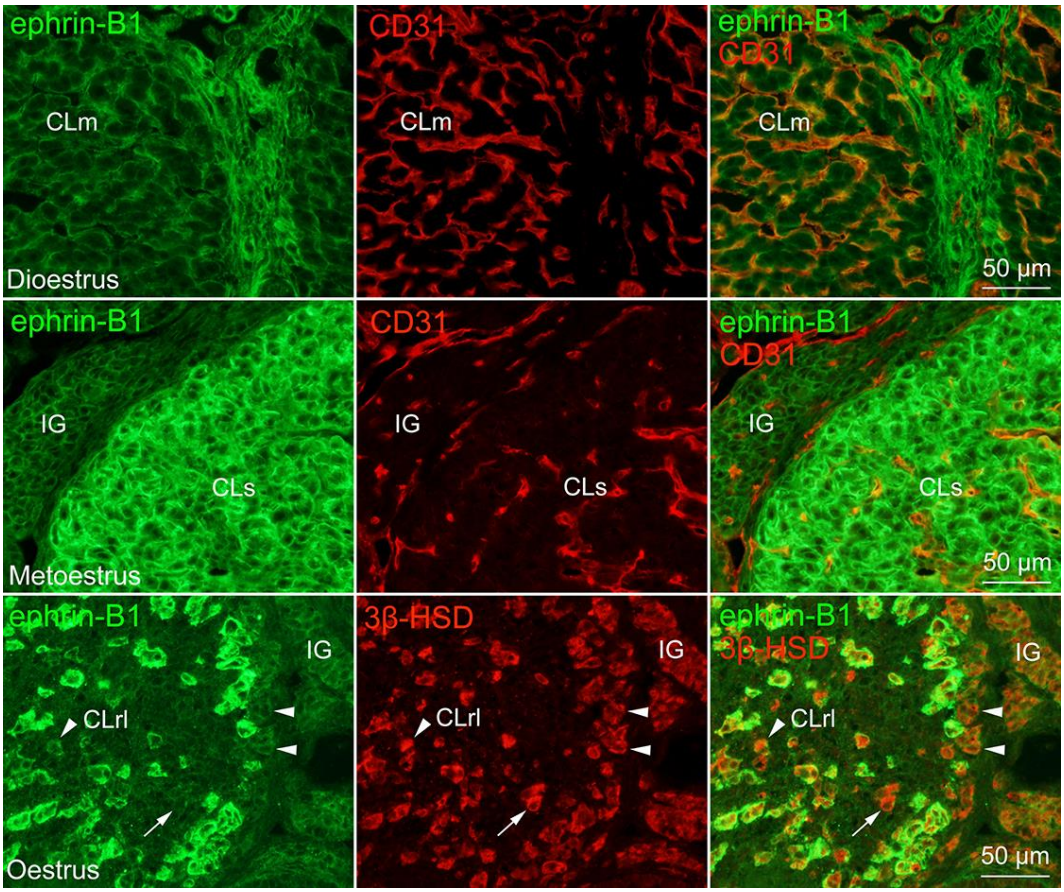
ephrin-B1
CLm
Dioestrus
CD31
CLm
ephrin-B1
CD31
CLm
50 µm
ephrin-B1
IG
CLs
Metoestrus
CD31
IG
CLs
ephrin-B1
CD31
IG
CLs
50 µm
ephrin-B1
IG
CLrl
Oestrus
3β-HSD
IG
CLrl
ephrin-B1
3β-HSD
IG
CLrl
50 µm

Fig. 2-3

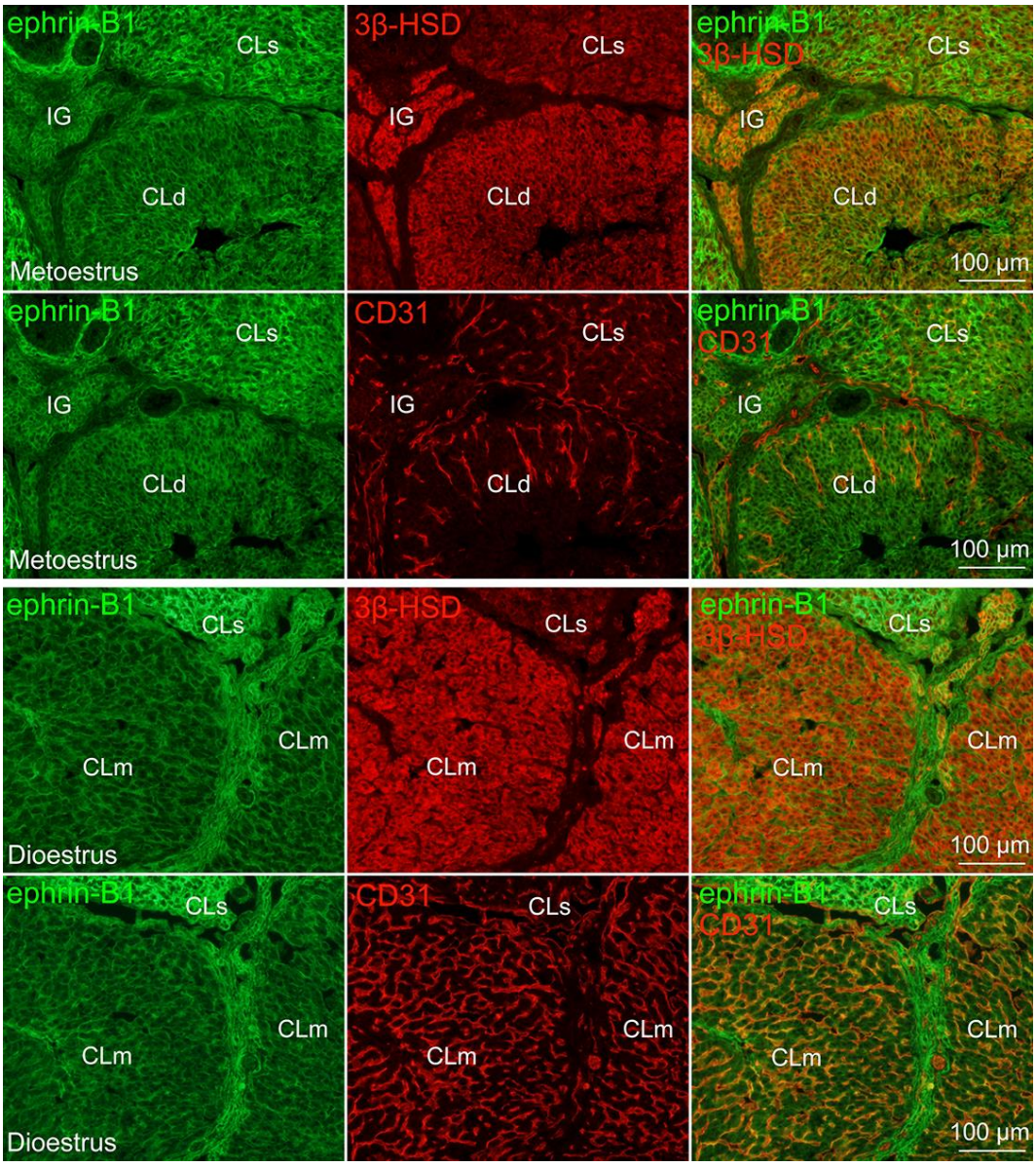
ephrin-B1
CLs
IG
CLd
Metoestrus
3β-HSD
CLs
IG
CLd
ephrin-B1
3β-HSD
CLs
IG
CLd
100 μm
ephrin-B1
CLs
IG
CLd
Metoestrus
CD31
CLs
IG
CLd
ephrin-B1
CD31
CLs
IG
CLd
100 μm
ephrin-B1
CLs
CLm
CLm
Dioestrus
3β-HSD
CLs
CLm
CLm
ephrin-B1
3β-HSD
CLs
CLm
CLm
100 μm
ephrin-B1
CLs
CLm
CLm
Dioestrus
CD31
CLs
CLm
CLm
ephrin-B1
CD31
CLs
CLm
CLm
100 μm

Fig. 2-4

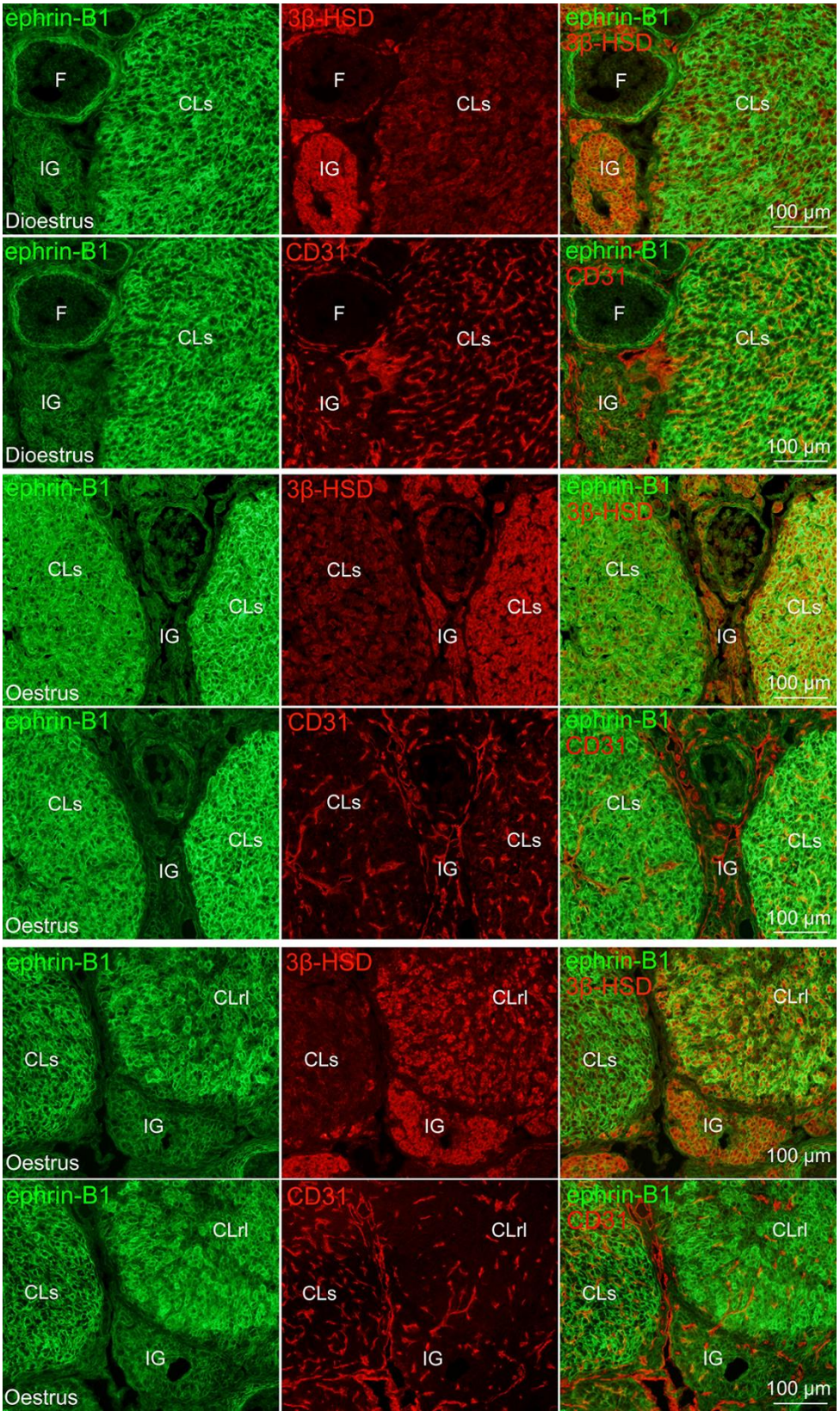

Fig. 2-5

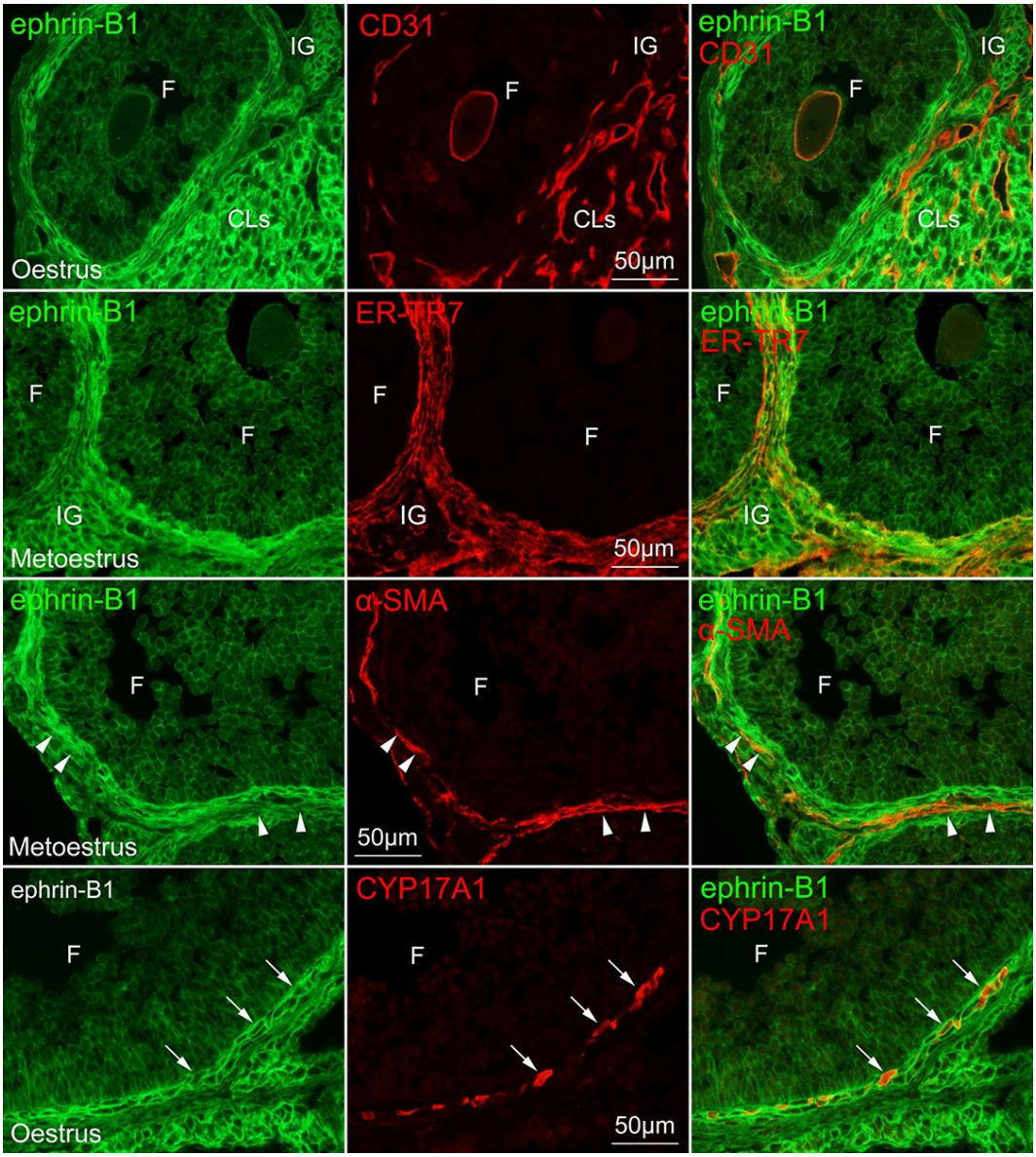
ephrin-B1
IG
F
CLs
Oestrus
CD31
IG
F
CLs
50μm
ephrin-B1
CD31
IG
F
CLs
ephrin-B1
F
F
IG
Metoestrus
ER-TR7
F
F
IG
50μm
ephrin-B1
ER-TR7
F
F
IG
ephrin-B1
F
Metoestrus
α-SMA
F
50μm
ephrin-B1
α-SMA
F
ephrin-B1
F
Oestrus
CYP17A1
F
50μm
ephrin-B1
CYP17A1
F

Fig. 2-6

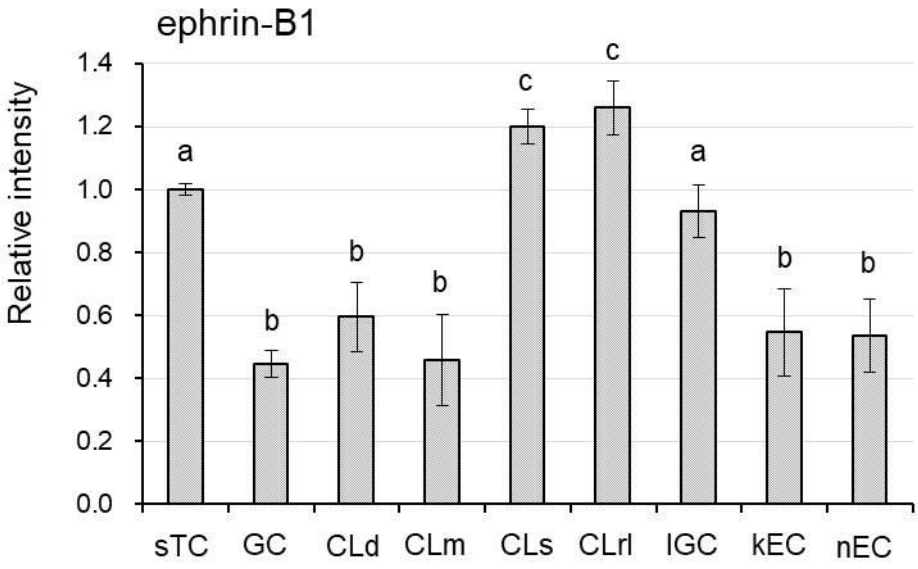
ephrin-B1
Relative intensity
1.4
1.2
1.0
0.8
0.6
0.4
0.2
0.0
a
b
b
b
c
c
a
b
b
sTC
GC
CLd
CLm
CLs
CLrl
IGC
kEC
nEC

Fig. 2-7

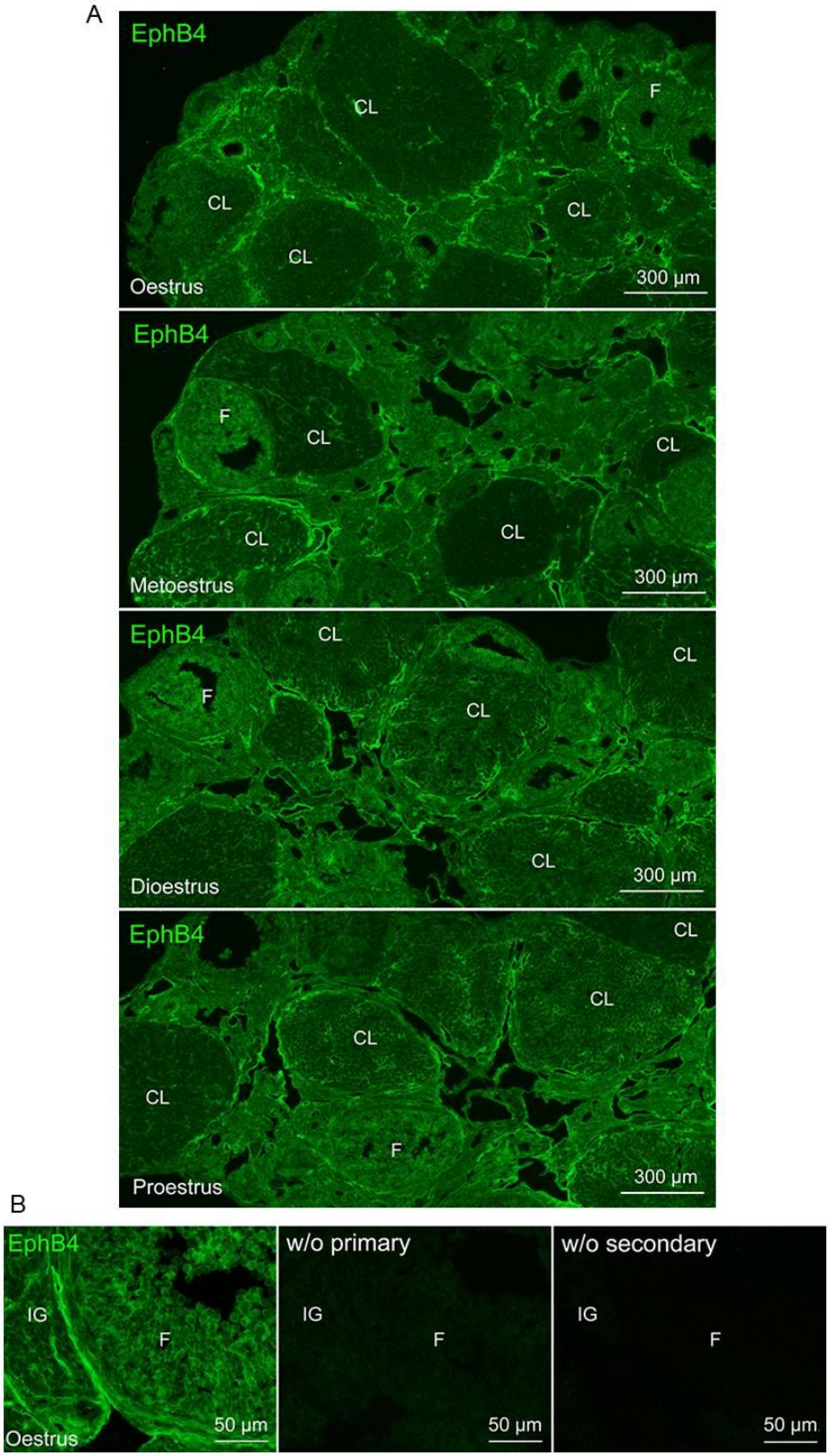
A
EphB4
CL
F
CL
CL
CL
Oestrus
300 µm
EphB4
F
CL
CL
CL
CL
Metoestrus
300 µm
EphB4
CL
CL
F
CL
CL
Dioestrus
300 µm
EphB4
CL
CL
CL
CL
F
Proestrus
300 µm
B
EphB4
IG
F
Oestrus
50 µm
w/o primary
IG
F
50 µm
w/o secondary
IG
F
50 µm

Fig. 2-8

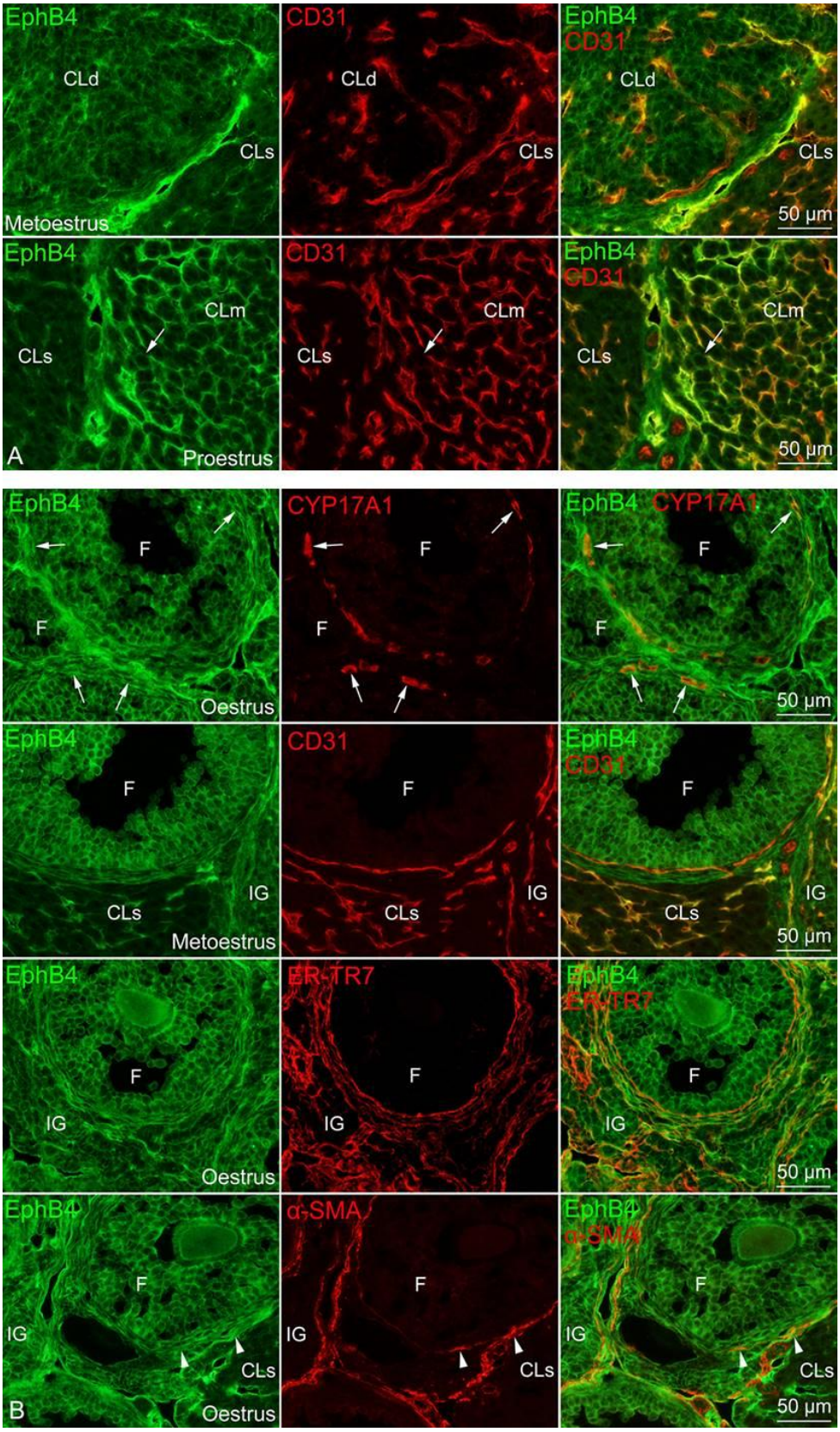
EphB4
CLd
CLs
Metoestrus
CD31
CLd
CLs
EphB4
CD31
CLd
CLs
50 µm
EphB4
CLm
CLs
A
Proestrus
CD31
CLm
CLs
EphB4
CD31
CLm
CLs
50 µm
EphB4
F
F
Oestrus
CYP17A1
F
F
EphB4 CYP17A1
F
F
50 µm
EphB4
F
IG
CLs
Metoestrus
CD31
F
IG
CLs
EphB4
CD31
F
IG
CLs
50 µm
EphB4
F
IG
Oestrus
ER-TR7
F
IG
EphB4
ER-TR7
F
IG
50 µm
EphB4
F
IG
CLs
B
Oestrus
α-SMA
F
IG
CLs
EphB4
α-SMA
F
IG
CLs
50 µm

Fig. 2-9

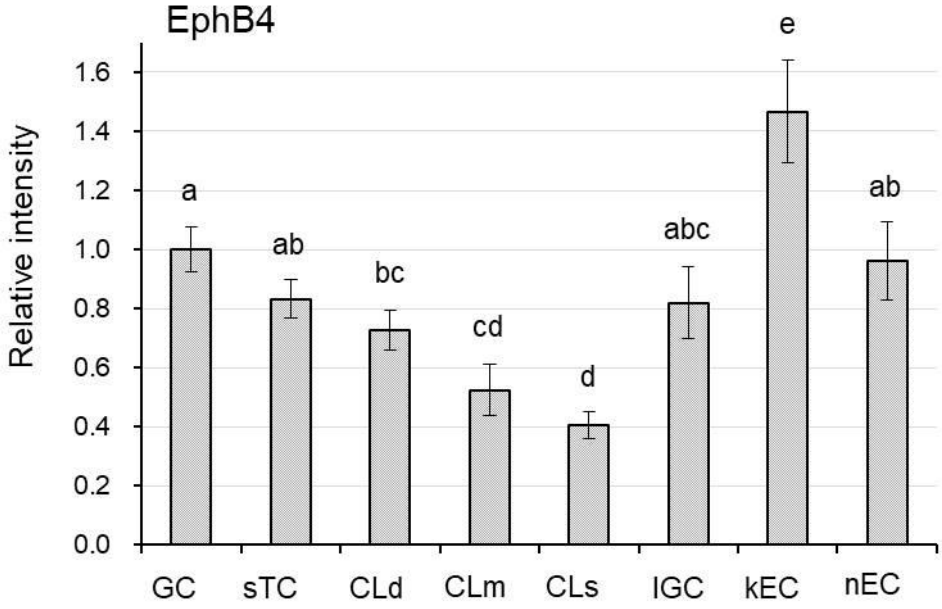
EphB4
Relative intensity
1.6
1.4
1.2
1.0
0.8
0.6
0.4
0.2
0.0
a
ab
bc
cd
d
abc
e
ab
GC
sTC
CLd
CLm
CLs
IGC
kEC
nEC

Fig. 2-10

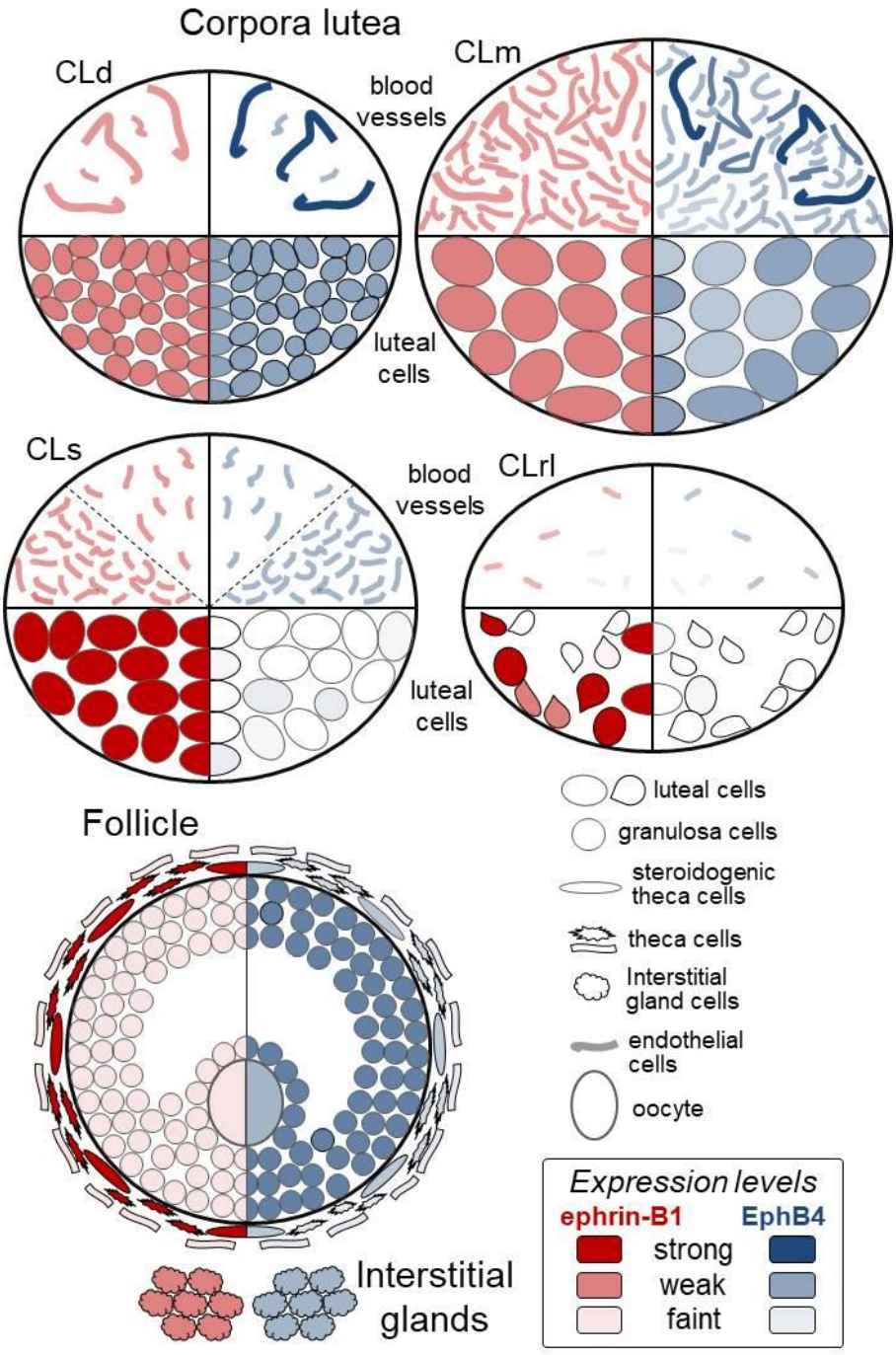
Corpora lutea
CLd
blood vessels
CLm
luteal cells
CLs
blood vessels
CLrl
luteal cells
Follicle
Interstitial glands
luteal cells
granulosa cells
steroidogenic theca cells
theca cells
Interstitial gland cells
endothelial cells
oocyte
Expression levels
ephrin-B1
EphB4
strong
weak
faint

Fig. 2-11

Figure legends

Figure 2-1

RT-PCR amplification of *EFNB1* and *EPHB4* mRNA from mouse ovaries. **A**) Transcripts of *EFNB1* and *EPHB4* were detected in naturally cycling mouse ovaries at all oestrous cycle phases. **B**) Densitometric quantification of mRNA expression levels for *EFNB1* and *EPHB4* from four independent experiments, normalised to *GAPDH*, is shown as means ± SD.

Figure 2-2

A) Immunofluorescence micrographs showing overviews of ephrin-B1 immunoreactivity in naturally cycling mouse ovaries at the four oestrous cycle phases. Note that ephrin-B1 immunoreactivity is similar among both interstitial glands and follicles but appreciably different among corpora lutea. **B**) No specific immunoreactivity in the ovary is almost invisible in the control sections without the primary or secondary antibodies. Serial sections were used for the control experiments. Specific immunoreactivities of ephrin-B1 are shown by comparing test sections immunostained with the primary antibody and secondary antibody (left panel) with the control sections without the primary (middle panel) or secondary antibodies (right panel). Micrographs of the same regional frame were taken with the same exposure time (356 ms). CL, corpus luteum; IG, interstitial gland.

Figure 2-3

Double immunofluorescence micrographs showing ephrin-B1 expressing cells in corpora lutea. Sections were stained with the indicated antibodies. Ephrin-B1 immunoreactivity is localised in 3β-HSD-positive luteal cells and interstitial gland cells as well as CD31-positive vascular endothelial cells. Note that ephrin-B1 immunoreactivity varies in corpora lutea: weak (CLm in top panels) and strong (CLs in middle panels) in major component cells except

CD31-positive cells, i.e. luteal cells. Moreover, ephrin-B1 immunoreactivity varies in certain corpus lutea (CLrl in bottom panels): strong, weak (arrowheads), and/or faint/negative (arrow) in 3β-HSD-positive luteal cells. CLm, temporally mature corpus luteum; CLrl, regressing corpus luteum of a late phase; CLs, corpus luteum of the previous cycles; IG, interstitial gland.

Figure 2-4

Double immunofluorescence micrographs showing ephrin-B1 immunoreactivity in corpora lutea by double staining with ephrin-B1 and 3β-HSD and ephrin-B1 and CD31 in serial sections. Note that ephrin-B1 immunoreactivity in 3β-HSD-positive luteal cells is weak in the corpus luteum showing developing features (CLd) and temporally mature features (CLm). CLd, developing corpus luteum; CLm, temporally mature corpus luteum; CLs, corpus luteum of the previous cycles; IG, interstitial gland.

Figure 2-5

Double immunofluorescence micrographs showing ephrin-B1 immunoreactivity in corpora lutea by double staining with ephrin-B1 and 3β-HSD and ephrin-B1 and CD31 in serial sections. Ephrin-B1 immunoreactivity is strong in the corpora lutea of the previous cycles (CLs) composed of weakly-3β-HSD-positive cells largely present and CD31-positive blood vessels of a high density (top two panels) as well as those composed of strongly- or weakly-3β-HSD-positive cells largely occupied and CD31-positive blood vessels of a low density (middle two panels). Ephrin-B1 immunoreactivity varies in luteal cells in the corpus luteum showing regressing features of the late phase (CLrl) composed of strongly-3β-HSD-positive cells distributed somewhat sparsely and CD31-positive blood vessels of a prominently low density (bottom two panels). CLrl, regressing corpus luteum; CLs, corpus luteum of the previous cycles; F, follicle; IG, interstitial gland.

Figure 2-6

Double immunofluorescence micrographs showing ephrin-B1-expressing cells in follicles. Sections were stained with the indicated antibodies. Note that ephrin-B1 immunoreactivity is (1) faint but substantial in granulosa cells; (2) weak/faint in the cells of the thin outer layer (theca externa, comprising α-SMA-positive smooth muscle cells [arrowheads]) and (3) strong in the cells of the thick inner layer of theca folliculi (theca interna, where CYP17A1-positive steroidogenic theca cells were located sparsely [arrows]). CLs, corpus luteum of the previous cycles; F, follicle; IG, interstitial gland.

Figure 2-7

Densitometric semi-quantitative fluorescence intensities showing ephrin-B1 immuno-reactivities in the steroidogenic cells as well as in vascular endothelial cells in corpora lutea. Because ephrin-B1 immunoreactivities were similar among theca folliculi (theca interna cells) as well as during the four oestrous cycle phases, ephrin-B1 immunoreactivity in the steroidogenic theca cells was used as controls to compare their expression levels among the steroidogenic cells and vascular endothelial cells. Single and double fluorescence micrographs (2070 × 1548 pixels; captured by a 20X objective lens) having follicles were selected. The expression levels of ephrin-B1 were determined from >5 micrographs per target steroidogenic cells/vascular endothelial cells; the fluorescence intensities of >10 regions (30 × 30 pixels/region) in each micrograph were measured in targeting cells as well as steroidogenic theca cells as controls using ImageJ image processing programme. The relative intensities to the controls were calculated from the average intensities of each micrograph. All values represent means ± SD. The differences in the ephrin-B1 expression levels between the target cells were evaluated, and *P*-values < 0.05 were considered statistically significant. sTC,

steroidogenic theca cells; GC, granulosa cells; CLd, luteal cells in developing corpora lutea; CLm, luteal cells in temporally mature corpora lutea; CLs, luteal cells in regressing/non-functional corpora lutea; CLrl, luteal cells in regressing corpora lutea of a late phase; IGC, interstitial gland cells; kEC, endothelial cells of thick blood vessels in corpora lutea; nEC endothelial cells of thin blood vessels in the corpora lutea.

Figure 2-8

A) Immunofluorescence micrographs showing overviews of EphB4 immunoreactivity in naturally cycling mouse ovaries at the four oestrous cycle phases. Note that EphB4 immunoreactivity is largely similar among follicles but appreciably different among corpora lutea. **B**) No specific immunoreactivity in the ovary is almost invisible in the control sections without the primary or secondary antibodies. Serial sections were used for the control experiments. Specific immunoreactivities of EphB4 are shown by comparing test sections immunostained with the primary antibody and secondary antibody (left panel) with the control sections without the primary (middle panel) or secondary antibodies (right panel). Micrographs of the same regional frame were taken with the same exposure time (400 ms). F, follicle; IG, interstitial gland.

Figure 2-9

Double immunofluorescence micrographs showing EphB4 expression in corpora lutea, follicles and interstitial glands. Sections were stained with the indicated antibodies. **A)** EphB4 immunoreactivity in corpora lutea. EphB4 immunoreactivity in CD31-positive vascular endothelial cells is strong in the stroma and varies in and among corpora lutea. EphB4 immunoreactivity in major cells except CD31-positive cells in corpora lutea, i.e. luteal cells also varies among corpora lutea: it is substantial/weak in small luteal cells in the developing

corpus luteum (CLd) as well as in large luteal cells (arrow) in the temporally mature corpus luteum (CLm); it is faint/negative in CD31-negative cells in the regressing/non-functional corpora lutea of the previous cycle composed of CD31-positive blood vessels of a low density (CLs). **B)** EphB4 immunoreactivity in follicles and interstitial glands. EphB4 immunoreactivity is prominent in granulosa cells and oocytes. EphB4 is substantially expressed in cells composed of theca folliculi, i.e. in CYP17A1-positive steroidogenic theca cells (arrows), CD31-positive vascular endothelial cells, ER-TR7-positive fibroblastic cells and α-SMA-positive smooth muscle cells (arrowheads). CLs, CLd & CLm, corpus luteum; F, follicle; IG, interstitial gland.

Figure 2-10

Densitometric semi-quantitative fluorescence intensities showing EphB4 immunoreactivities in the steroidogenic cells as well as in vascular endothelial cells in corpora lutea. Because EphB4 immunoreactivities were similar among granulosa cells of follicles as well as during the four oestrous cycle phases, EphB4 immunoreactivity in granulosa cells was used as controls to compare their expression levels among the steroidogenic cells and vascular endothelial cells. Single and double fluorescence micrographs (2070 × 1548 pixels; captured by a 20X objective lens) having follicles were selected. The expression levels of EphB4 were determined from >5 micrographs per target steroidogenic cells/vascular endothelial cells; the fluorescence intensities of >10 regions (30 × 30 pixels/region) in each micrograph were measured in targeting cells as well as granulosa cells as controls using ImageJ image processing programme. The relative intensities to the controls were calculated from the average intensities of each micrograph. All values represent means ± SD. The differences in the EphB4 expression levels between the target cells were evaluated, and *P*-values < 0.05 were considered statistically significant. sTC, steroidogenic theca cells; GC, granulosa cells;

CLd, luteal cells in developing corpora lutea; CLm, luteal cells in temporally mature corpora lutea; CLs, luteal cells in regressing/non-functional corpora lutea; IGC, interstitial gland cells; kEC, endothelial cells of thick blood vessels in corpora lutea; nEC, endothelial cells of thin blood vessels in the corpora lutea.

Figure 2-11

Schematic drawings of steroidogenic cells and vasculatures in corpora lutea illustrating the expression levels and patterns of ephrin-B1 and EphB4 in the ovary. The upper and lower half of corpora lutea show expression patterns of vascular endothelial cells and luteal cells, respectively. The left and right sides of the drawing show expression patterns of ephrin-B1 and EphB4, respectively. Expression levels were depicted by shading of the dark red (ephrin-B1) and navy colours (EphB4): deep, relatively strong; pale, weak; very pale, faint. CLd, a developing corpus luteum composed of strongly-/weakly-3β-HSD-positive small cells and CD31-positive thick blood vessels of a low density running towards the centre; CLm, a temporally mature corpus luteum composed of strongly-3β-HSD-positive large luteal cells and CD31-positive blood vessels of a prominently high density; CLrl, a regressing corpus luteum of a late phase composed of strongly 3β-HSD-positive cells distributed sparsely and CD31-positive blood vessels of a prominently low density; CLs, a regressing/non-functional corpus luteum of the previous cycle composed of strongly 3β-HSD-positive luteal cells and CD31-positive blood vessels of a low density as well as those composed of weakly 3β-HSD-positive luteal cells and CD31-positive blood vessels at a low or high density.

Chapter 3

Expression and localisation of ephrin-B1 and EphB4

in adrenal glands of male and female mice

Introduction

Eph receptors and ephrins have been implicated in the physiology and homeostasis of normal adult tissues and organs (Pasquale, 2008; Miao and Wang, 2009). In adult epithelial tissues, Eph/ephrin signaling is implicated in maintaining epithelial integrity and homeostasis in a variety of epithelia such as the small and large intestine, epidermis, and mammary glands (Miao and Wang, 2009; Perez White and Getsios, 2014). Ogawa and his colleagues showed the expression levels and functions of EphB and ephrin-B in the rodent gastric glandular and non-glandular epithelia and suggested that EphB and ephrin-B are involved in (1) maintenance of the gastric epithelial unit (Ishii et al., 2011; Ogawa et al., 2011; Uchiyama et al., 2015) and (2) formation of an epithelial boundary at the squamocolumnar junction along the proximal-to-distal axis of the gastric epithelia (Ogawa et al., 2013). They also showed that the ephrin-B1- and EphB2/B4-predominant expression compartments appear alternately along the excurrent system in the testis and epididymis, which is lined with the tubule/ductule/duct-specific epithelia. Thus, these findings indicate that the Eph/ephrin cell-cell communication system operates extensively in the epithelia of adult tissues and organs to maintain their integrity and homeostasis.

The adrenal gland is a representative steroidogenic organ in which cortical epithelial cells produce corticosteroids. The adrenal gland consists of the medulla and cortex, and cortical progenitor cells located in the periphery migrate centripetally and repopulate the inner cortical zones upon differentiation (Belloni et al., 1978; Spencer et al., 1999). The adrenal cortex is composed of three zones as the zona glomerulosa (zG), zona fasciculata (zF), and zona reticularis (zR) in many mammals while the cortex is composed of zG and zF in aged mice (Pihlajoki et al., 2015). The adrenal cortex in young mice contains an ephemeral layer between zF and adrenal medulla known as the x-zone (xZ) (Hirokawa and Ishikawa, 1974;

Morohashi and Zubair, 2011). The murine xZ develops after birth and regresses in the male at puberty and in the female during the first pregnancy (Holmes and Dickson, 1971; Kim and Choi, 2020). Cells in the xZ are derived from the foetal adrenal gland and involved in progesterone catabolism (Zubair et al., 2006; Hershkovitz et al., 2007).

Based on recent findings showing co-expression of ephrin-B1 and EphB4 in adult and foetal Leydig cells (Gofur et al., 2020), the author hypothesised that "ephrin-B1 and EphB4 are co-expressed in sex steroid-producing cells" and demonstrated co-expression of ephrin-B1 and EphB4 in all the steroidogenic cells of naturally cycling mouse ovaries in Chapter 2. Thus the author further hypothesised that "ephrin-B1 and EphB4 are co-expressed in not only sex steroid-producing cells but also corticosteroid-producing cells". To the best of the author's knowledge, however, the expression and localisation of ephrin-B1 ligands and EphB4 receptors have not been reported in the adrenal gland. Thus the author examined ephrin-B1 and EphB4 expression and localisation in the male and female mouse adrenal glands to test this hypothesis in Chapter 3.

Materials and Methods

Animals

ICR mice of both sexes, aged 5 and 8 weeks and kept under standard housing (12 h light/12 h dark cycle; 22–23°C with 50 -55% humidity) and feeding conditions were used for reverse transcription-polymerase chain reaction (RT-PCR) and immunofluorescence staining experiments. A total of 16 mice (8 males and 8 virgin females) were used in this study. Mice were sacrificed by cervical dislocation or an overdose of pentobarbital (Nacalai Tesque, Kyoto, Japan), and the right and left adrenal glands were collected. Animal experimentation protocols were approved by the Animal Research Committee of Osaka Prefecture University (approval number: 21-26).

Total RNA extraction and semi-quantitative RT-PCR analysis

Total RNA was isolated from the right adrenal gland in male and female ICR mice aged 8 weeks (4 males and 4 females) using TRizol reagent (Invitrogen, Carlsbad, CA, USA), and RT-PCR analysis was performed as previously described (Gofur et al., 2020). In brief, 1 μg total RNA was transcribed into first-strand cDNA using M-MLV reverse transcriptase, RNase H^- (Promega, Madison, WI, USA), and an oligo $(dT)_{18}$ primer, according to the manufacturer's instructions. For the detection of endogenous *EFNB1*, *EPHB4,* and *GAPDH*, 0.5 μL of the 25-μL reaction mixture was amplified with Taq DNA polymerase (TaKaRa Ex Taq HS; TaKaRa Bio Inc., Otsu, Japan) using the reverse-transcribed cDNA as template. The primer pairs and thermal cycling conditions used for PCR amplification are shown in Table 3-1. The PCR cycle number was determined based on the linear amplification range obtained with samples in males when the expression levels were almost similar between male and female mice. The RT reaction was omitted for negative controls. PCR products were separated on 1.5% agarose gels and visualised by ethidium bromide staining. The expression levels of amplified *EFNB1* and *EPHB4* mRNAs were determined from four independent experiments, normalised to the levels of *GAPDH* mRNA as an internal control (amplified over 23 cycles), and compared the male and female.

Antibodies

Goat polyclonal antibodies against the mouse ephrin-B1 extracellular domain (AF473) and the mouse EphB4 extracellular domain (AF446) were purchased from R&D Systems, Inc. (Minneapolis, MN, USA). A rabbit polyclonal antibody against 3β-HSD, as a marker of steroidogenic cells (Hershkovitz et al., 2007), was purchased from Trans Genic Inc. (KO607; Kobe, Japan). A rat monoclonal antibody against mouse CD31, as a marker of vascular

endothelial cells (Gofur and Ogawa, 2019), was obtained from BD Biosciences (553370; Franklin Lakes, NJ, USA). Alexa Fluor 488-conjugated donkey anti-goat IgG (A-11055), Alexa Fluor 594-conjugated donkey anti-rabbit IgG (A-21207), and Alexa Fluor 594-conjugated donkey anti-rat IgG (A-21209) were obtained from molecular probes, Inc. (Eugene, OR, USA).

Immunofluorescence staining

The left adrenal glands of male and female mice aged 5 and 8 weeks were fixed with 10 % formalin in phosphate-buffered saline (PBS) for ~4 h at 4°C. Adrenal glands aged 8 weeks were used for ephrin-B1 staining and those aged 5 weeks were used for EphB4 stainings because relatively strong autofluorescence from the cortical cells appeared only in sections of 8 weeks old mice immunostained with the EphB4 antibody. After washing with PBS, the adrenal glands were immersed in 30 % sucrose in PBS overnight and mounted in optimum cutting temperature compound (Sakura Fine Technical Co., Ltd., Tokyo, Japan). Then, 6 µm-thick cryostat sections were cut and used for immunofluorescence staining. Single or double immunofluorescence staining was performed as previously described (Ogawa et al., 2011). Briefly, cryostat sections were incubated in a humid chamber with 1% BSA in PBS (BSA-PBS), followed by incubation with single or mixed primary antibodies at a concentration 1 µg/mL (anti-ephrin-B1, anti-3ß-HSD), 4 µg/mL (anti-EphB4), and 1:2,000 (anti-CD31) for 1.5 h at 32°C. After washing with PBS, the sections were incubated with (1) Alexa Fluor 488-conjugated donkey anti-goat IgG (5 µg/mL) in BSA-PBS, (2) a mixture of Alexa Fluor 488-conjugated donkey anti-goat IgG (5 µg/mL) and Alexa Fluor 594-conjugated donkey anti-rabbit IgG (5 µg/mL), or (3) a mixture of Alexa Fluor 488-conjugated donkey anti-goat IgG (5 µg/mL) and Alexa Fluor 594-conjugated donkey anti-rat IgG (5 µg/mL) for 30 min at 32°C. The sections were washed with PBS, mounted with PermaFluor (Thermo Scientific), and

photographed under an inverted fluorescence microscope (IX71; Olympus, Tokyo, Japan) using a digital camera (DP72; Olympus) controlled by the manufacturer's software (DP2-BSW; Olympus). Green fluorescence and red fluorescence of the same field were captured using 10X and 20X objective lenses (IX71, Olympus), and fluorescence micrographs were merged using Adobe Photoshop (San Jose, CA, USA).

Semi-quantitative analyses on ephrin-B1 and EphB4 immunofluorescence intensities in steroidogenic cells

Relative immunofluorescence intensities of ephrin-B1 and EphB4 were semi-quantitatively analysed in steroidogenic cells as well as in vascular endothelial cells by densitometry. As ephrin-B1 and EphB4 immunoreactivities in the male and female were quite similar among endothelial cells distributed in the zF beneath the zG and the medulla, respectively, these immunoreactivities were used as controls to compare their expression levels among the cortical parenchymal cells. Double fluorescence micrographs (2070 × 1548 pixels; captured by a 20X objective lens) in which those cortical parenchymal cells and vasculatures appeared in were selected. The expression levels of ephrin-B1 and EphB4 were determined from >5 micrographs per target cortical parenchymal cells/vascular endothelial cells in the male and female; the fluorescence intensities of >10 regions (30 × 30 pixels/region) in each micrograph were measured using ImageJ image processing programme (National Institutes of Health, Bethesda, MD, USA). The relative intensities to the controls (those of endothelial cells distributed in the zF beneath the zG for ephrin-B1 and distributed in the medulla for EphB4) were calculated from the average intensities of each micrograph.

Statistical analysis

Statistical analyses were performed with Microsoft Excel and statistical software available online (http://statpages.info/anova1sm.html). Differences in *EFNB1* and *EPHB4* mRNA expression levels among the adrenal glands of males and female mice as well as the differences in the ephrin-B1 and EphB4 expression levels between the target cells were evaluated by one-way ANOVA, followed by Tukey's HSD post-hoc analysis. *P*-values less than 0.05 were considered significant. All values represent means ± SD.

Results

mRNA expression of ephrin-B1 and EphB4

To investigate the relative expression levels of ephrin-B1and EphB4 in the adrenal gland of male and virgin female mice aged 8 weeks, semi-quantitative RT-PCR was performed. The transcripts of *EFNB1* and *EPHB4* were detected in both male and female adrenal glands (Fig. 3-1A). The relative expression levels of *EFNB1* and *EPHB4* were similar between the male and female (Fig. 3-1B). These findings indicate that ephrin-B1 and EphB4 expressions are likely as common in males and females.

Ephrin-B1 immunoreactivity

The cortex is composed of zG and zF in adult mice (Pihlajoki et al., 2015) but zG, zF, and xZ as an additional zone beneath zF in young mice (Hirokawa and Ishikawa, 1974; Morohashi and Zubair, 2011). The murine xZ, where cortical cells derived from the foetal adrenal gland reside, develops after birth and regresses in the male at puberty (4-6 weeks old of age) and in the female during the first pregnancy (Holmes and Dickson, 1971; Zubair et al., 2006; Hershkovitz et al., 2007; Kim and Choi, 2020).

Ephrin-B1 immunoreactivity was prominent in the whole cortex and faint/negative in the medulla in the adult male. By contrast in the adult virgin female, ephrin-B1

immunoreactivity was prominent in the outer half of the cortex and gradually decreased towards the medulla (Fig. 3-2). Thus, the author used a 3β-HSD antibody to label cortical cells to identify the cortical regions in both the male and female (Fig. 3-3). A boundary between 3β-HSD-positive and -negative regions clearly appeared in the adrenal gland of male mice. By contrast, a boundary between 3β-HSD-positive and -negative regions irregularly/nonlinearly appeared in that of female mice. A boundary by ephrin-B1-positive and negative regions corresponded to that by 3β-HSD-positive and negative regions, i.e. a histological boundary between the cortex and medulla in male mice while not in female mice: ephrin-B1 immunoreactivity was different in the adrenal cortex labeled by 3β-HSD immunoreactivity between the male and female. Ephrin-B1 immunoreactivity was strong in the zG and bottom region of zF (zFb), and weak/faint in the middle region of zF (zFm) of the cortex in the male while strong in the zG, weak/faint in the middle (zFm) and bottom region (zFb) of zF as well as in xZ in the female (Fig. 3-3).

Because the adrenal cortex is chiefly composed of steroidogenic parenchymal cells and capillary endothelial cells, the author used the double staining of ephrin-B1 and CD31, a marker protein of vascular endothelial cells clearly to identify ephrin-B1-positive cells. Ephrin-B1 immunoreactivity was localised in CD31-positive endothelial cells and CD31-negative cells. These CD31-negative cells were large/round/oval/quadrangular in shape and arranged in epithelial structures. According to the morphology and distribution pattern, these CD31-negative cells were likely steroidogenic parenchymal cells in the cortex of both the male and female. Ephrin-B1 immunoreactivity was strong and similar among CD31-positive endothelial cells distributed in the zF beneath the zG in male and female while weak in CD31-positive endothelial cells distributed in other regions in the cortex and faint/negative in those distributed in the medulla (Fig. 3-4). Thus, the author defined ephrin-B1 immunoreactivity similar to/greater than that observed in endothelial cells distributed in the zF beneath the zG as

'strong', and immunoreactivity less than that in the endothelial cells as 'weak' or 'faint'. Ephrin-B1 immunoreactivity was strong in CD31-negative cortical parenchymal cells in the zG and in a narrow region of the zF adjacent to the zG and the medulla, and weak/faint in CD31-negative cortical parenchymal cells in the middle region of the zF in male mice (Fig.3-4). By contrast, ephrin-B1 immunoreactivity was strong in CD31-negative cortical parenchymal cells in the zG and weak/faint in cortical parenchymal cells in the zF and zX in female mice (Fig. 3-4). These qualitative expression levels of ephrin-B1 immunoreactivity (strong, weak, faint) largely corresponded to relative fluorescence intensities that were semi-quantitatively determined from cellular fluorescence intensities in CD31-negative cortical parenchymal cells (steroidogenic cells) and vascular endothelial cells distributed in the zF beneath the zG and normalised to/compared with those of the endothelial cells as controls (standard), via densitometric quantification in both male and female (Fig. 3-5). These findings indicate that ephrin-B1 was substantially expressed in all parenchymal cells (steroidogenic cells) in the adrenal cortex of both the male and female but their expression level varied in parenchymal cells among zones/regions in the cortex as well as between the male and female.

EphB4 immunoreactivity

EphB4 immunoreactivity in the male at puberty and the virgin female at puberty was prominent in the whole cortex and faint/negative in the medulla except vasculatures (Fig. 3-6). EphB4 immunoreactivity other than vasculatures was detected largely in 3β-HSD-positive regions corresponding to the cortex of both the male and female (Fig. 3-7). Because the cortex is composed of parenchymal cells and capillary endothelial cells as major cells, the author used the double staining EphB4 and CD31 labeling vascular endothelial cells to identify EphB4-positive cells. EphB4 immunoreactivity was localised in CD31-positive endothelial cells and CD31-negative large round/oval/quadrangular cells arranged in epithelial structures,

i.e. steroidogenic parenchymal cells in the cortex of both the male and the virgin female. EphB4 immunoreactivity was strong and similar among CD31-positive endothelial cells distributed in the cortex and medulla in male and female (Fig. 3-8). Thus, the author defined EphB4 immunoreactivity similar to that observed in endothelial cells distributed in the medulla as 'strong', and immunoreactivity less than that in the endothelial cells as 'weak' or 'faint'.

EphB4 immunoreactivity was slightly different in CD31-negative parenchymal cells among zones in the adrenal cortex of both male and female mice (Fig. 3-8): EphB4 immunoreactivity in CD31-negative parenchymal cells was weak in the zG, and weak/faint in the zF of both the male and female. Moreover, EphB4 immunoreactivity was weak in CD31-negative parenchymal cells in the zX of the virgin female (Fig. 3-8). EphB4 immunoreactivity was slightly different in CD31-positive endothelial cells among zones in the adrenal cortex of both male and female mice. EphB4 immunoreactivity was weak in CD31-positive endothelial cells in zG while strong in other zones in the cortex and medulla in both male and female mice (Fig. 3-8).These qualitative expression levels of EphB4 immunoreactivity (strong, weak, faint) largely corresponded to relative fluorescence intensities that were semi-quantitatively determined from cellular fluorescence intensities in CD31-negative cortical parenchymal cells (steroidogenic cells) and vascular endothelial cells distributed in the medulla in both male and female and normalised to/compared with those of the endothelial cells as controls (standard), via densitometric quantification (Fig. 3-9).

Overall findings indicate that ephrin-B1 and EphB4 were substantially co-expressed in parenchymal cells (steroidogenic cells) distributed in all zones of the adrenal cortex in both the male and virgin female, but their expression level varied in parenchymal cells among zones in the cortex. Ephrin-B1 and EphB4 expression patterns and levels in parenchymal cells of the adrenal cortex in the male and female mice are illustrated in Fig. 3-10.

Discussion

Eph receptors and ephrins are membrane protein that acts as a cell-cell communication system. In adult epithelial tissues, Eph/ephrin signalling is implicated in maintaining epithelial integrity and homeostasis in a variety of epithelia such as the small and large intestine, epidermis, and mammary glands (Miao and Wang, 2009; Perez White and Getsios, 2014). Recently Gofur et al. showed that both foetal and adult Leydig cells commonly co-expressed ephrin-B1 and EphB4 in the mouse testis (Gofur and Ogawa, 2019; Gofur et al., 2020). Based on this, the author hypothesised that ephrin-B1 and EphB4 are co-expressed ubiquitously in sex steroid-producing cells in gonads. To test this hypothesis, the author examined ephrin-B1 and EphB4 expression in naturally cycling mouse ovaries and found that both molecules were co-expressed in all types of sex steroid-producing cells in the ovaries in Chaper 2. In Chapter 3, the author hypothesised co-expression of ephrin-B1 and EphB4 not only in sex steroid-producing cells of gonads but also in corticosteroid-producing cells in the adrenal gland, and tested this hypothesis. Ephrin-B1 and EphB4 mRNA were similarly expressed in the adrenal gland of male and female mice. A previous report showing mRNA expression of several ephrins and Eph receptors including ephrin-B1 and EphB4 in the rat adrenal gland supports this finding (Brennan et al., 2008). The author also found that ephrin-B1 and EphB4 were co-localised in cortical parenchymal cells distributed in all zones of the adrenal cortex as well as in vascular endothelial cells distributed in the adrenal cortex in the male and female mice. This is the first study clearly characterising ephrin-B1 and EphB4 expressing cells in adrenal glands of mammals. Moreover, the present findings confirmed the author's hypothesis. Because all types of steroidogenic cells residing in the adult and developing testis (Gofur and Ogawa, 2019; Gofur et al., 2020), the adult ovary (Chaper 2) and the adrenal gland co-expressed ephrin-B1 and EphB4, co-expression of ephrin-B1 and EphB4 is likely common in

steroidogenic cells, and thus, possibly represents a good marker to identify steroidogenic cells even in extra-gonadal and extra-adrenal organs/tissues.

In the intestine, epithelial stem cells are located in the bottom of the crypt, proliferate and differentiate into several types of enterocytes, and migrate from the bottom of the crypt towards the tip of the villus (Batlle et al., 2002). It is accepted that epithelial compartments formed by a ephrin-B-dominant expressing cell region (villus region) and a EphB-dominant expressing cell region (crypt region) appeared along villus-crypt axis of the intestinal epithelium due to repulsive signals arising from the contact between EphB-expressing and ephrin-B-expressing enterocytes (Batlle et al., 2002). Similarly to the intestinal epithelial cell arrangement, a previous study showed that progenitors of cortical parenchymal cells reside in the surface layer of the adrenal glands (capsule); undifferentiated proliferative cells located in the surface layer of the adrenal cortex undergo differentiation into cortical parenchymal cells and migrate inward along with their differentiation; this cortical migration gives rise to the sequential zonation along with the alteration of cortical cell phenotypes, i.e., mineralocorticoid-producing cells in the zG, glucocorticoid-producing cells in the zF and sex steroid-producing cells in the zR of human adrenal gland (Pihlajoki et al., 2015). Moreover, Brennan et al. showed that EphA2 and EphA3 were localised in cortical cells of the zG and ephrin-A1, A2, A3 and A4 mRNA were expressed in the rat adrenal gland (Brennan et al., 2008). Refering to the enterocyte organization mechanism found by Batlle et al. (Batlle et al., 2002), Brennan et al. speculated that EphA/ephrin-A signalling is possibly involved in the maintenance of adrenocortical zone formation. The author found that ephrin-B1 and EphB4 were localised in cortical parenchymal cells and vascular/capillary endothelial cells distributed in the adrenal cortex, and their expression levels varied among the zones of the adrenal cortex in the male and female mice. Moreover, ephrin-B1/EphB4-expression compartments appeared not only within cortical parenchymal cells but also within capillaries

in the cortex in both the male and female: (1) In cortical cells, ephrin-B1 and EphB4 immunoreactivity were strong and weak, respectively, in the zG, and weak/faint in the zF in both the male and female. Moreover, ephrin-B1 immunoreactivity was strong in the bottom part of the zF in the male and weak/faint in the xZ in the female while EphB4 immunoreactivity was weak/faint in the bottom part of the zF in the male and weak in the xZ in the female. (2) In endothelial cells, ephrin-B1 and EphB4 immunoreactivity were weak in those distributed in the zG, and very strong in those distributed at the boundary between the zG and the zF in both the male and female. Ephrin-B1 in the male was strong in endothelial cells distributed in the zF and weak/faint in those distributed at the boundary between the zF and the medulla while that in the female was strong in those distributed in the upper region of the zF, and weak/faint in the lower region of the zF and the xZ. EphB4 was strong in endothelial cells distributed in the zF in the male and female and very strong in those distributed at the boundary between the zF and the medulla in the male and in the xZ of the female. These findings may indicate that ephrin-B1/EphB4 signalling arise within cortical cells relatively strong in the zG and weak in zF in both the male and female as well as strong in the bottom of the zF of the male and in the xZ of the female. These findings may also indicate that ephrin-B1/EphB4 signalling arised from the contact between cortical cells and capillary endothelial cells is likely strong at the boundary between the zG and zF as well as at the boundary between the zF and the medulla in the male and in the xZ in the female. Thus it is very intriguing that ephrin-B1/EphB4 signalling arising from the contact among cortical cells as well as between cortical cells and capillary endothelial cells involves in the zone formation of the cortical cells. Further studies will be required to examine this hypothesis.

Summary

This study represents the first detailed expression/localisation analysis of ephrin-B1 and EphB4 in the adrenal gland of male and female mice. The author found that ephrin-B1 and EphB4 are co-expressed in steroidogenic cells of all types present in the adrenal gland. Ephrin-B1 immunoreactivity was strong in cortical parenchymal cells in the zG and a narrow region of the zF adjacent to the zG and the medulla, and weak/faint in cortical parenchymal cells in the middle region of the zF in the male. By contrast, EphB4 immunoreactivity was slightly different in parenchymal cells in the adrenal cortex of both male and female mice: EphB4 immunoreactivity in parenchymal cells was weak in the zG, and weak/faint in the zF of both the male and female as well as weak in the xZ of the virgin female. Although further investigation is required to provide in-depth clarification of the role of these molecules in the adrenal glands, the expression pattern of ephrin-B ligand and EphB receptor may represent benchmarks for examining steroidogenic cells in the adrenal glands.

Table 3-1. Primers and cycle numbers for PCR amplification					
Primer			Product size (bp)	Annealing temp. (°C)	Cycle number
ephrin-B1	Forward	5′-TGCTTGATCCCAATGTACTG-3′	520	55.0	29
	Reverse	5′-CGGAGCTTGAGTAGTAGGAC-3′			
EphB4	Forward	5′-AGCCCCAAATAGGAGACGAG-3′	540	57.9	34
	Reverse	5′-GGATAGCCCATGACAGGATC-3′			
GAPDH	Forward	5′-ACTTTGGCATTGTGGAAGGG-3′	375	58.3	23
	Reverse	5′-AGTGGGAGTTGCTGTTGAAG-3′			

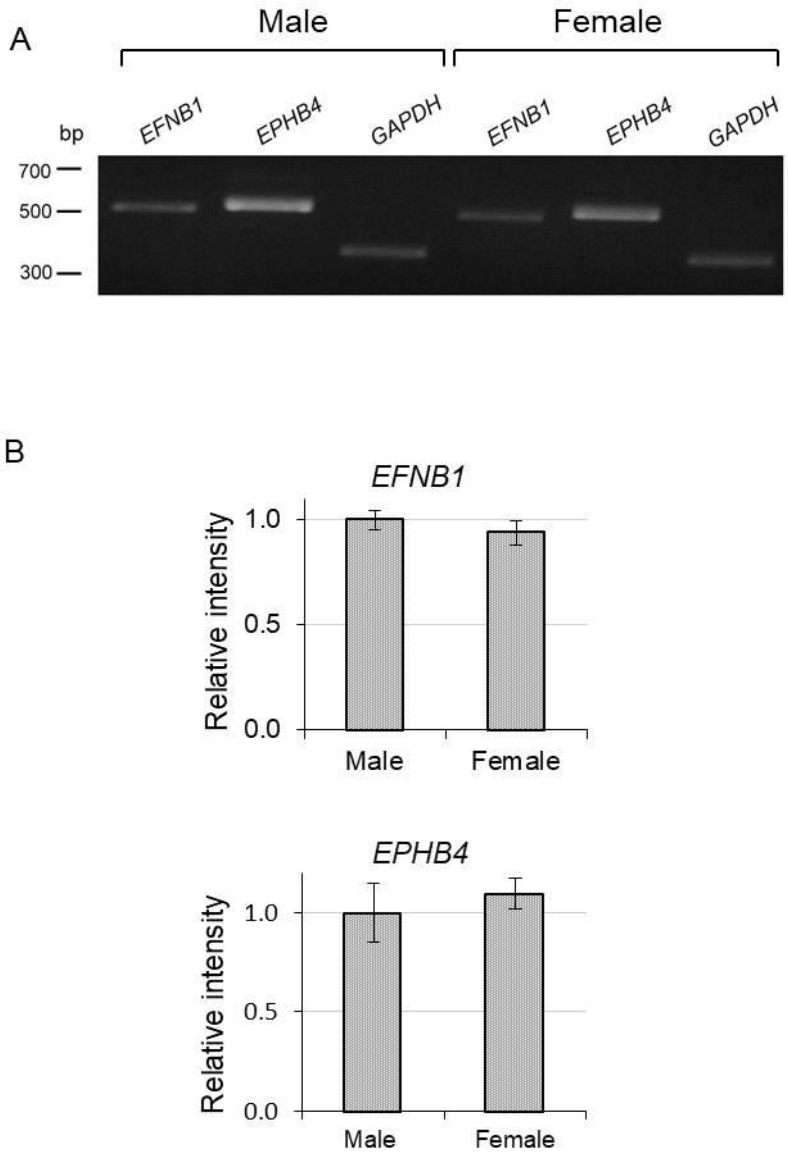
A
Male
Female
bp
EFNB1
EPHB4
GAPDH
EFNB1
EPHB4
GAPDH
700
500
300
B
EFNB1
Relative intensity
1.0
0.5
0.0
Male
Female
EPHB4
Relative intensity
1.0
0.5
0.0
Male
Female

Fig. 3-1

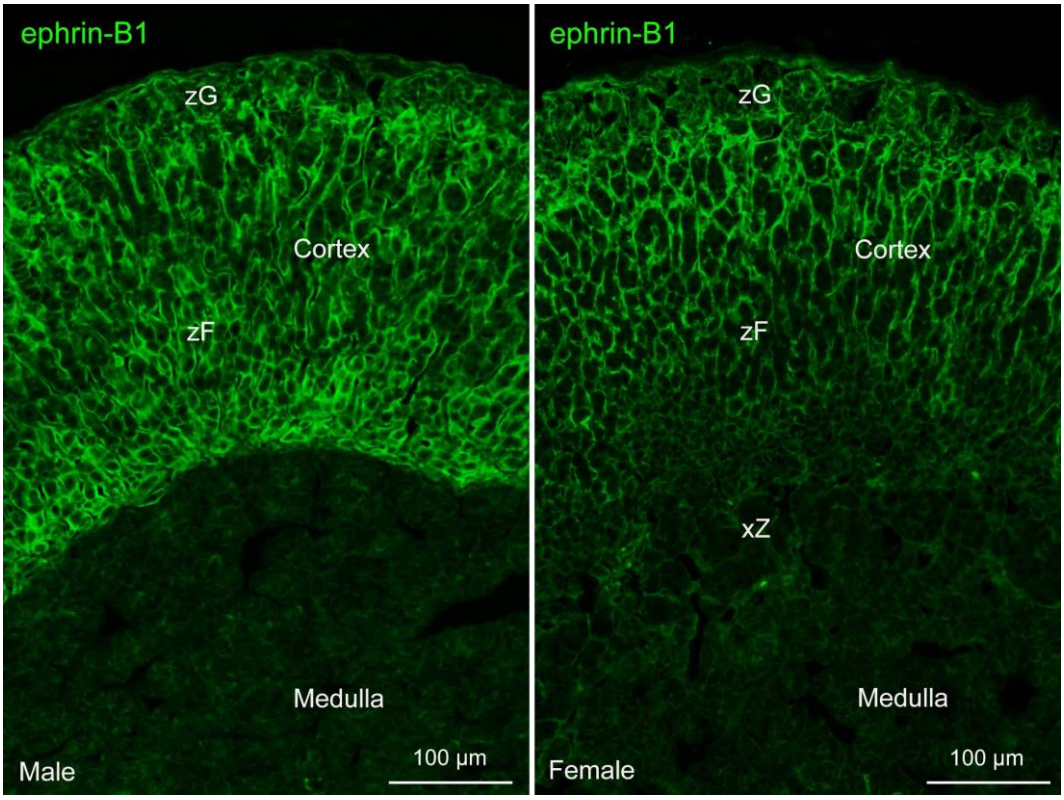
ephrin-B1
zG
Cortex
zF
Medulla
Male
100 µm
ephrin-B1
zG
Cortex
zF
xZ
Medulla
Female
100 µm

Fig. 3-2

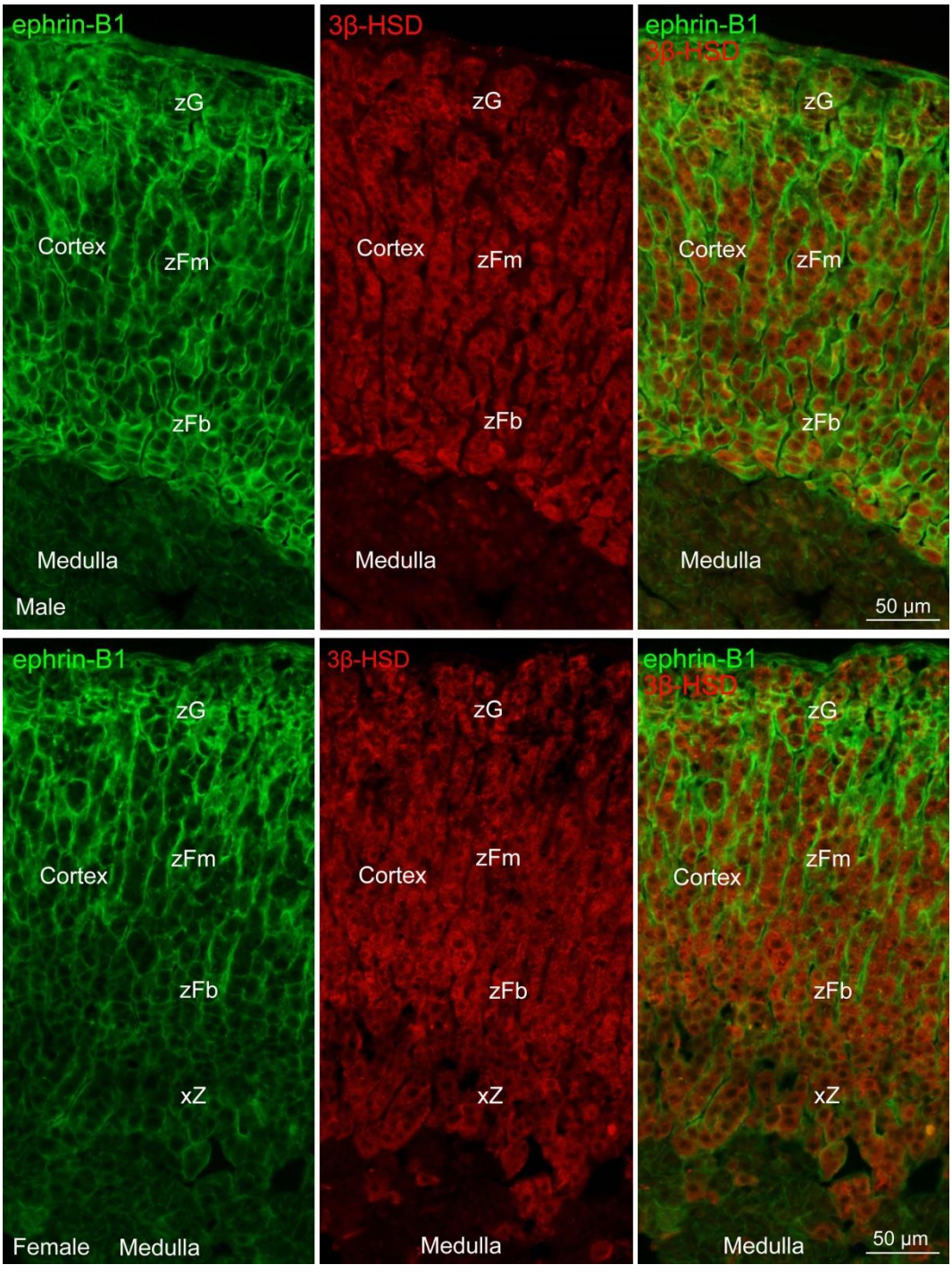
ephrin-B1
zG
Cortex
zFm
zFb
Medulla
Male
3β-HSD
zG
Cortex
zFm
zFb
Medulla
ephrin-B1
3β-HSD
zG
Cortex
zFm
zFb
Medulla
50 μm
ephrin-B1
zG
Cortex
zFm
zFb
xZ
Female
Medulla
3β-HSD
zG
Cortex
zFm
zFb
xZ
Medulla
ephrin-B1
3β-HSD
zG
Cortex
zFm
zFb
xZ
Medulla
50 μm

Fig. 3-3

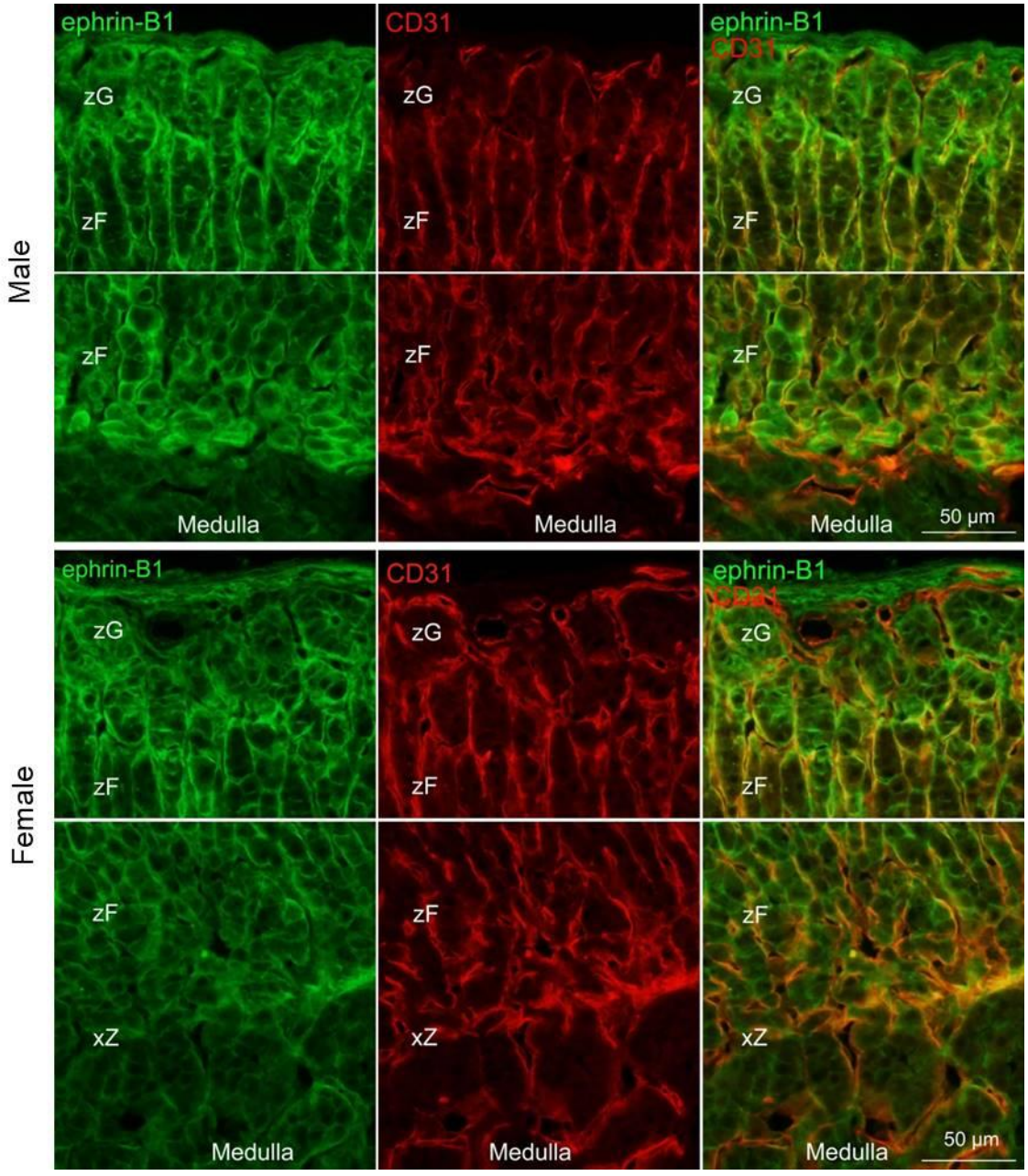

Fig. 3-4

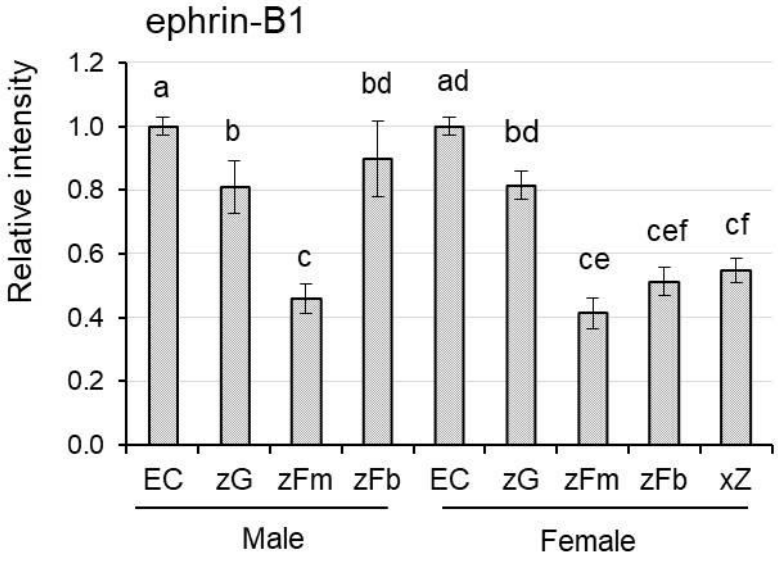
ephrin-B1
Relative intensity
1.2
1.0
0.8
0.6
0.4
0.2
0.0
a
b
c
bd
ad
bd
ce
cef
cf
EC
zG
zFm
zFb
EC
zG
zFm
zFb
xZ
Male
Female

Fig. 3-5

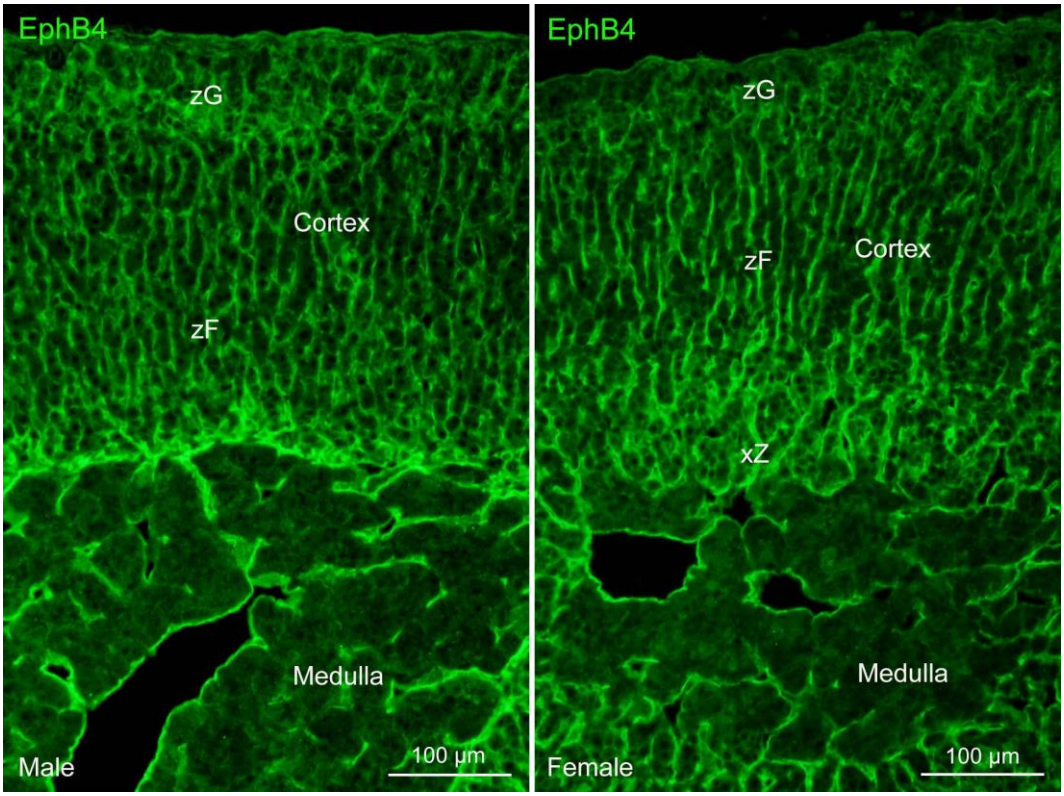
EphB4
zG
Cortex
zF
Medulla
Male
100 µm
EphB4
zG
zF
Cortex
xZ
Medulla
Female
100 µm

Fig. 3-6

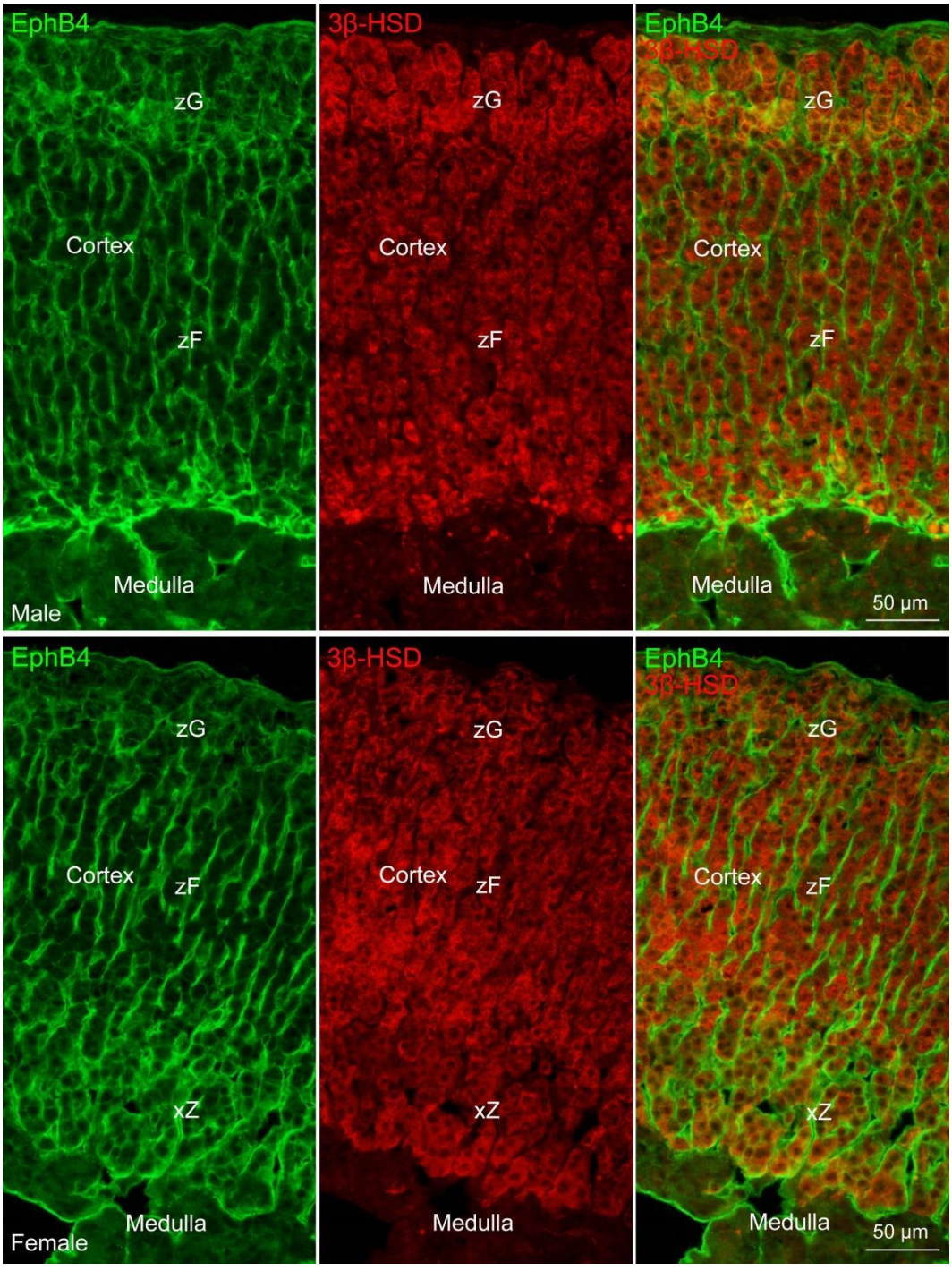
EphB4
zG
Cortex
zF
Medulla
Male
3β-HSD
zG
Cortex
zF
Medulla
EphB4
3β-HSD
zG
Cortex
zF
Medulla
50 μm
EphB4
zG
Cortex
zF
xZ
Medulla
Female
3β-HSD
zG
Cortex
zF
xZ
Medulla
EphB4
3β-HSD
zG
Cortex
zF
xZ
Medulla
50 μm

Fig. 3-7

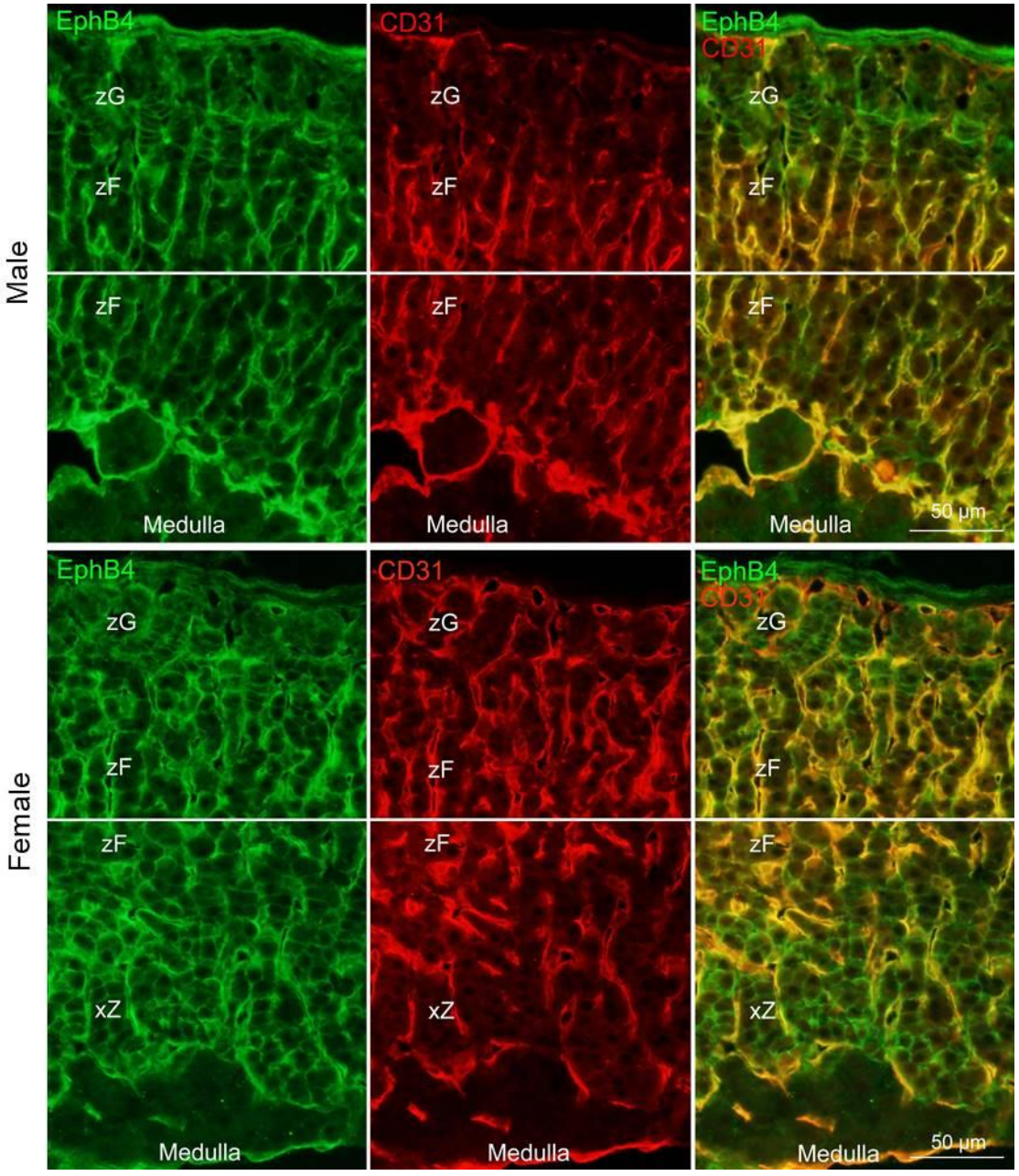

Fig. 3-8

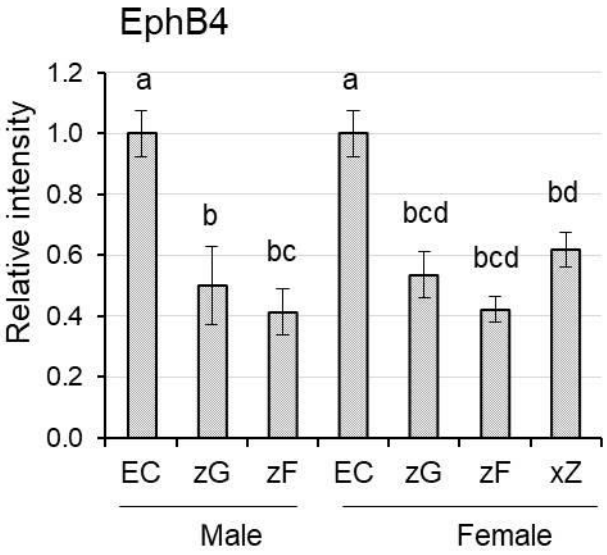
EphB4
Relative intensity
1.2
1.0
0.8
0.6
0.4
0.2
0.0
a
b
bc
a
bcd
bcd
bd
EC
zG
zF
EC
zG
zF
xZ
Male
Female

Fig. 3-9

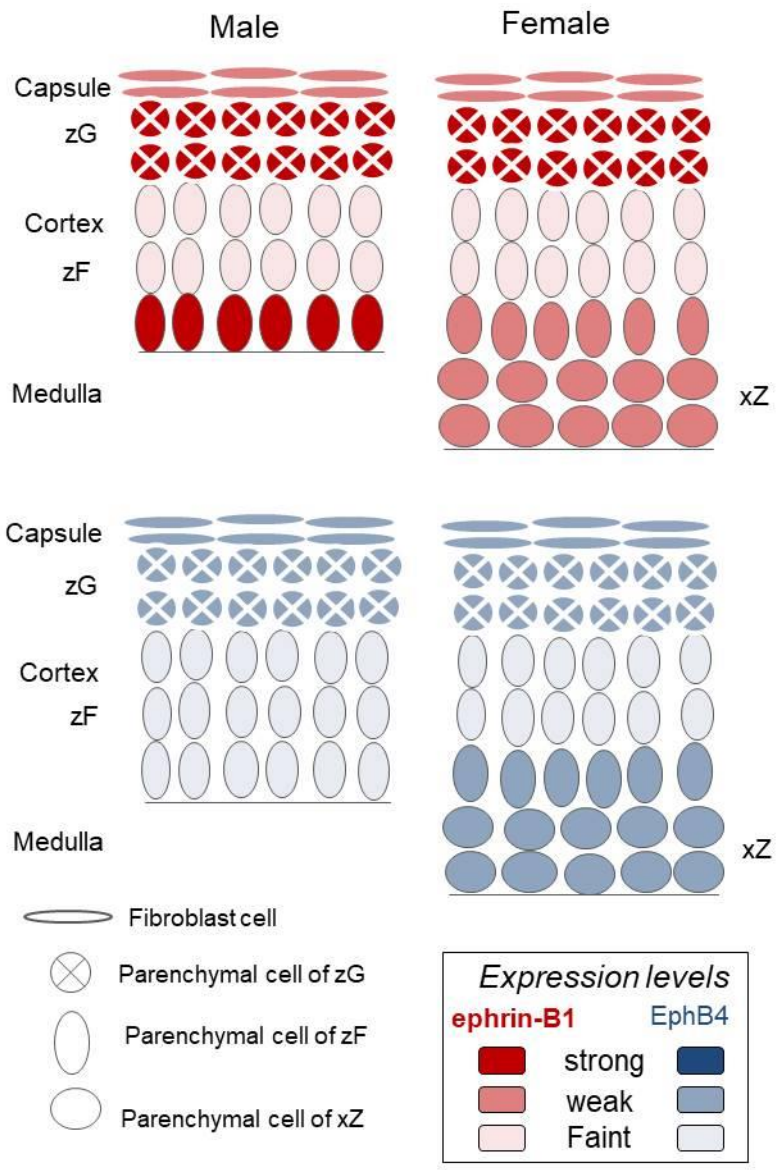
Male
Female
Capsule
zG
Cortex
zF
Medulla
xZ
Capsule
zG
Cortex
zF
Medulla
xZ
Fibroblast cell
Parenchymal cell of zG
Parenchymal cell of zF
Parenchymal cell of xZ
Expression levels
ephrin-B1
EphB4
strong
weak
Faint

Fig. 3-10

Figure legends

Figure 3-1

RT-PCR amplification of *EFNB1* and *EPHB4* mRNA from adrenal glands of male and female mice aged 8 weeks. **A**) Transcripts of *EFNB1* and *EPHB4* were detected in male and female mouse adrenal glands. **B**) Densitometric quantification of mRNA expression levels for *EFNB1* and *EPHB4* from four independent experiments, normalised to *GAPDH*, are shown as means ± SD

Figure 3-2

Immunofluorescence micrographs showing overviews of ephrin-B1 immunoreactivity in the adrenal glands of male and female mice aged 8 weeks. Note that ephrin-B1 immunoreactivity is prominent in the whole cortex and faint/negative in the medulla in the adult male. By contrast in the adult virgin female, ephrin-B1 immunoreactivity is prominent in the outer half of the cortex and gradually decreases towards the medulla where the immunoreactivity is faint/almost negative. zG, zona glomerulosa; zF, zona fasciculata; xZ, x-zone.

Figure 3-3

Double immunofluorescence micrographs showing ephrin-B1 and 3β-HSD immunoreactivity in the adrenal gland of male and female mice aged 8 weeks. Sections were stained with the indicated antibodies. Note that a clear boundary by ephrin-B1-positive and -negative regions corresponds to that by 3β-HSD-positive and -negative regions in the male adrenal gland, respectively. By contrast, a boundary lined by 3β-HSD-positive and -negative regions irregularly/nonlinearly appears in the female. Moreover, ephrin-B1 immunoreactivity varies in the adrenal cortex labeled by 3β-HSD immunoreactivity in both males and females. zG, zona glomerulosa; zFm, middle region of zF; zFb, bottom region of zF; xZ, x-zone.

Figure 3-4

Double immunofluorescence micrographs showing ephrin-B1 and CD31 immunoreactivity in the adrenal gland of male and female mice aged 8 weeks. Note that ephrin-B1 immunoreactivity is strong and similar among CD31-positive endothelial cells distributed in the zF beneath the zG in the male and female while weak in CD31-positive endothelial cells distributed in other regions in the cortex and faint/negative in those distributed in the medulla. Ephrin-B1 immunoreactivity is strong in CD31-negative cortical parenchymal cells in the zG and in a narrow region of the zF adjacent to the zG and the medulla, and weak/faint in CD31-negative cortical parenchymal cells in the middle region of the zF in male mice. By contrast, ephrin-B1 immunoreactivity is strong in CD31-negative cortical parenchymal cells in the zG, weak/faint in cortical parenchymal cells in the zF, and weak/faint in the xZ in female mice. zG, zona glomerulosa; zF,zona fasciculata; xZ, x-zone.

Figure 3-5

Densitometric semi-quantitative fluorescence intensities showing ephrin-B1 immunoreactivities in cortical parenchymal cells as well as in the vascular endothelial cells in the adrenal gland of male and female mice aged 8 weeks. Because ephrin-B1 immunoreactivities were similar among capillary endothelial cells distributed in the zF beneath the zG in both the male and female adrenal gland. Ephrin-B1 immunoreactivity in the endothelial cells was used as controls (standard) to compare ephrin-B1 expression levels among cortical parenchymal cells. Single and double fluorescence micrographs (2070 × 1548 pixels; captured by a 20X objective lens) were selected. The expression levels of ephrin-B1 were determined from >5 micrographs per target cells/vascular endothelial cells; the fluorescence intensities of >10 regions (30 × 30 pixels/region) in each micrograph were measured in target cells using the ImageJ image processing programme. The average

intensities of capillaries used as control were calculated from 10 micrographs (5 micrographs from males and 5 micrographs from females). All values represent means ± SD. The differences in ephrin-B1 expression levels between the target cells were evaluated, and *P*-values < 0.05 were considered statistically significant. EC, endothelial cells distributed in the zF beneath the zG; zG, parenchymal cells in the zG; zFm, parenchymal cells in the middle region of the zF; zFb, parenchymal cells in the bottom region of the zF; xZ, parenchymal cells in the xZ in the female.

Figure 3-6

Immunofluorescence micrographs showing overviews of EphB4 immunoreactivity in the adrenal glands of male and female mice aged 5 weeks. Note that EphB4 immunoreactivity in the male and the virgin female mice is prominent in the whole cortex and faint/negative in the medulla except vasculatures. zG, zona glomerulosa; zF, zona fasciculata; xZ, x-zone.

Figure 3-7

Double immunofluorescence micrographs showing EphB4 and 3β-HSD immunoreactivity in the adrenal glands of male and female mice aged 5 weeks. Sections were stained with the indicated antibodies. EphB4 immunoreactivity other than vasculatures is detected largely in 3β-HSD-positive regions corresponding to the cortex of both the male and female. By contrast, EphB4 immunoreactivity is faint/negative in 3β-HSD-negative regions corresponding to the adrenal medulla except for vasculature in both the male and female. zG, zona glomerulosa; zF, zona fasciculata; xZ, x-zone.

Figure 3-8

Double immunofluorescence micrographs showing EphB4 and CD31 immunoreactivity in the adrenal glands of male and female mice aged 5 weeks. Note that EphB4 immunoreactivity is strong and similar among CD31-positive endothelial cells distributed in the cortex and medulla in males and females. EphB4 immunoreactivity in CD31-negative cortical parenchymal cells is weak in the zG, and faint/weak in the zF of both the male and female. EphB4 immunoreactivity was weak in CD31-negative cortical parenchymal cells in the xZ of the female. zG, zona glomerulosa; zF, zona fasciculata; xZ, x-zone.

Figure 3-9

Densitometric semi-quantitative fluorescence intensities showing EphB4 immunoreactivities in cortical parenchymal cells as well as in the vascular endothelial cells in the adrenal gland of of male and female mice aged 5 weeks. Because EphB4 immunoreactivities were similar among vascular endothelial cells distributed in the adrenal medulla of both the male and female. EphB4 immunoreactivity in the endothelial cells was used as controls (standard) to compare EphB4 expression levels among cortical parenchymal cells. Single and double fluorescence micrographs (2070 × 1548 pixels; captured by a 20X objective lens) were selected. The expression levels of EphB4 were determined from >5 micrographs per target cells/vascular endothelial cells; the fluorescence intensities of >10 regions (30 × 30 pixels/region) in each micrograph were measured in target cells using the ImageJ image processing programme. The average intensities of vasculatures in the medulla used as control were calculated from 10 micrographs (5 micrographs from males and 5 micrographs from females). All values represent means ± SD. The differences in the EphB4 expression levels between the target cells were evaluated, and *P*-values < 0.05 were considered statistically

significant. EC, endothelial cells distributed in the medulla; zG, parenchymal cells in the zG; zF, parenchymal cells in the zF; xZ, parenchymal cells in the xZ in the female.

Figure 3-10

Schematic drawings of the adrenal cortex illustrating the expression level and pattern of ephrin-B1 and EphB4 in cortical parenchymal cells of the male and female mice adrenal glands. The right and left shows the expression pattern of ephrin-B1 (upper) and EphB4 (lower) in cortical cells of the males and female, respectively. Expression levels were depicted by shading of the dark red (ephrin-B1) and navy colours (EphB4): Deep, relatively strong; pale, weak; very pale, faint. zG, cortical parenchymal cells in zona glomerulosa; zF, cortical parenchymal cells in zona fasciculata; xZ, cortical parenchymal cells in x-zone.

General discussion

Eph receptors and ephrins are membrane proteins that serve as a cell–cell communication system (Pasquale, 2005, 2010). Recently, Gofur et al. found that not only adult Leydig cells but also foetal Leydig cells co-express ephrin-B1 and EphB4 in the mouse testes (Gofur and Ogawa, 2019; Gofur et al., 2020). Based on this finding, the author speculated that steroidogenic cells may commonly co-express ephrin-B1 and EphB4, and therefore, examined their expression in the naturally cycling mouse ovaries as well as in the adrenal gland in this study.

The author found all steroidogenic cells in the ovaries co-express ephrin-B1 and EphB4. This finding represents the first detailed expression/localisation analysis of ephrin-B1 and EphB4 in the naturally cycling mammalian ovaries. The author also found that ephrin-B1 and EphB4 immunoreactivity are similar among the same type of steroidogenic cells except luteal cells in corpora lutea of naturally cycling mouse ovaries. Ephrin-B1 and EphB4 immunoreactivity in luteal cells were largely similar within single corpus luteum in most corpora lutea, but rather different between corpora lutea in an ovary section. Therefore, the author examined the maturation status of corpora lutea using a combination of 3β-HSD immunoreactivity in luteal cells and CD31-positive blood vessel densities and identified maturation statuses of corpora lutea in the naturally cycling mouse ovaries, and accordingly, corpora lutea were classified into four, i.e., CLd (developing corpora lutea frequently present in metoestrus), CLm (temporally mature corpora lutea frequently present in dioestrus and proestrus), CLs (regressing/non-functional corpora lutea of an older generation in the previous oestrous cycle), and CLrl (regressing small corpora lutea of a late phase present frequently in oestrus). Ephrin-B1 and EphB4 expression patterns in luteal cells are largely summarised as follows: ephrin-B1 expression in luteal cells was weak in developing and temporally mature corpora lutea of the current oestrous cycles and strong in regressing corpora lutea of the

previous cycle. On the contrary, EphB4 expression in luteal cells was weak in newly-formed corpora lutea of the current oestrous cycle and faint/negative in regressing corpora lutea of the previous cycles. The LH surge triggers the transformation of granulosa cells and steroidogenic theca cells into luteal cells and causes the regression of corpora lutea (luteolysis) (Stocco et al., 2007; Duffy et al., 2019); thus, these hormones may be candidate molecules to induce the upregulation of ephrin-B1 expression and downregulation of EphB4 in luteal cells. Further investigation is required to determine whether and how ephrin-B1 is upregulated and EphB4 is downregulated at these times.

In the adrenal glands, the author found all steroidogenic cells in the adrenal cortex co-express ephrin-B1 and EphB4. A previous report showed that mRNA of several ephrins and Eph receptors including ephrin-B1 and EphB4 are expressed in the rat adrenal gland and that EphA2 and EphA3 are localised in cortical cells of the zG (Brennan et al., 2008). Thus the author's finding represents the first detailed expression/localisation analysis of ephrin-B1 and EphB4 in the adrenal gland of male and female mammals. Based on the overall innunohisitochemical findings in the adult ovary (Chaper 2) and the adrenal glands of the male and female (Chaper 3), the author concluded that co-expressed ephrin-B1 and EphB4 is likely common in steroidogenic cells, and thus, possibly represents a good marker to identify steroidogenic cells even in extra-gonadal and extra-adrenal organs/tissues.

Conclusions

The author investigated the expression and localisation of ephrin-B1 and EphB4 in the naturally cycling mouse ovaries and the adrenal gland of the male and female mice especially to determine the ephrin-B1 and EphB4 co-expression as a novel marker for steroidogenic cells The results obtained as follows:

1. Ephrin-B1 and EphB4 were substantially co-expressed in all of 3β-HSD-positive cells in the ovaries, i.e. luteal cells, granulosa cells, steroidogenic theca cells, and interstitial gland cells while their expression levels varied in luteal cells of corpora lutea.
2. Ephrin-B1 expression in luteal cells was weak in developing and temporally mature corpora lutea (corpora lutea of the current oestrous cycle) and strong in regressing corpora lutea (corpora lutea of the previous cycles). By contrast, EphB4 expression in luteal cells was weak in corpora lutea of the current oestrous cycle and faint/negative in corpora lutea of the previous cycles.
3. Ephrin-B1 and EphB4 are co-expressed in all 3β-HSD-positive cortical parenchymal cells while their expression levels varied among zones on the adrenal cortex.
4. The present findings suggest that the co-expression of ephrin-B1 and EphB4 is likely a good marker to identify steroidogenic cells located not only in the ovary and the adrenal gland but also in diverse organs of mammalian adults and foetuses.

Acknowledgements

It is a great pleasure and honor of the author to acknowledge a group of extremely well people who made my doctoral thesis to appear. The author feels proud to express his deepest sense of gratitude, sincere appreciation, profound regards, and immense indebtedness to his reverend supervisor Professor Dr. Kazushige Ogawa for his research planning, scholastic guidance, sympathetic supervision, utmost desire, valuable suggestions, wise criticism, constructive and constant inspiration throughout the entire period of the study, research work and in preparation of this manuscript. The author really wants to thank him from the bottom of his heart for being such a friendly and cooperative supervisor. The author would like to express the highest gratefulness and deepest sense of gratitude to Associate professor Dr. Takayuki Nakajima for his kind co-operation, generous help, and valuable comments throughout the entire period of the study as well as in reviewing this thesis. The author would like to give sincere thanks to Dr. Takashi Tanida for his critical and insightful comments and encouragement. The author would like to give sincere thanks to Professor Dr. Niritoshi Kawate and Professor Dr. Mitsuru Kuamura for their critical and insightful comments and encouragement in reviewing this thesis. The author is thankful to The Ministry of Education, Culture, Sports, Science, and Technology (MEXT) of Japan government for providing scholarships for his doctoral study and will remain grateful to Osaka Prefecture University for providing all the nice academic facilities and qualified staff. The author is really grateful to Md. Royhan Gofur, Tsurutani Mayu,Yamauchi Sawako,Tanaka Yuki,Yukari Kohara, Horie Haruka for their sincere support in his research work and many other important issues during in working period in Japan. The author is also thankful to all lab members who were always friendly and helpful. Thanks are extended to all of the well-wishers for their direct and indirect inspiration and help in completing this research work. Last but no way to the least, the author wishes to express ever grateful and immensely indebted to his respected parents, his idol of family and daily life late Md. Sultan Mia, his inspiration, strength, and source of eternal happiness Dr. Shakila Sultana, affectionate brothers and sisters for their heartiest blessings, affectionate feelings, encouragement, and all sorts of sacrifices for the author's higher education and successful completion of this humble research work.

The Author

March, 2022

References

Adams RH, Wilkinson GA, Weiss C, Diella F, Gale NW, Deutsch U, Risau W, Klein R. 1999. Roles of ephrinB ligands and EphB receptors in cardiovascular development: demarcation of arterial/venous domains, vascular morphogenesis, and sprouting angiogenesis. Genes Dev 13:295-306.

Adu-Gyamfi EA, Czika A, Liu TH, Gorleku PN, Fondjo LA, Djankpa FT, Ding YB, Wang YX. 2021. Ephrin and Eph receptor signaling in female reproductive physiology and pathology†. Biol Reprod 104:71-82.

Batlle E, Henderson JT, Beghtel H, van den Born MM, Sancho E, Huls G, Meeldijk J, Robertson J, van de Wetering M, Pawson T, Clevers H. 2002. Beta-catenin and TCF mediate cell positioning in the intestinal epithelium by controlling the expression of EphB/ephrinB. Cell 111:251-263.

Belloni AS, Mazzocchi G, Meneghelli V, Nussdorfer GG. 1978. Cytogenesis in the rat adrenal cortex: evidence for an ACTH-induced centripetal cell migration from the zona glomerulosa. Arch Anat Histol Embryol 61:195-205.

Brennan CH, Chittka A, Barker S, Vinson GP. 2008. Eph receptors and zonation in the rat adrenal cortex. J Endocrinol 198:185-191.

Buensuceso AV, Deroo BJ. 2013. The ephrin signaling pathway regulates morphology and adhesion of mouse granulosa cells in vitro. Biol Reprod 88:25.

Buensuceso AV, Son AI, Zhou R, Paquet M, Withers BM, Deroo BJ. 2016. Ephrin-A5 Is Required for Optimal Fertility and a Complete Ovulatory Response to Gonadotropins in the Female Mouse. Endocrinology 157:942-955.

Cohen PE, Zhu L, Pollard JW. 1997. Absence of colony stimulating factor-1 in osteopetrotic (csfmop/csfmop) mice disrupts estrous cycles and ovulation. Biol Reprod 56:110-118.

Duffy DM, Ko C, Jo M, Brannstrom M, Curry TE. 2019. Ovulation: Parallels With Inflammatory Processes. Endocr Rev 40:369-416.

Duncan WC, Rodger FE, Illingworth PJ. 1998. The human corpus luteum: reduction in macrophages during simulated maternal recognition of pregnancy. Hum Reprod 13:2435-2442.

Egawa M, Yoshioka S, Higuchi T, Sato Y, Tatsumi K, Fujiwara H, Fujii S. 2003. Ephrin B1 is expressed on human luteinizing granulosa cells in corpora lutea of the early luteal phase: the possible involvement of the B class Eph-ephrin system during corpus luteum formation. J Clin Endocrinol Metab 88:4384-4392.

Fraser HM, Wulff C. 2003. Angiogenesis in the corpus luteum. Reprod Biol Endocrinol 1:88.

Gaytan F, Morales C, Leon S, Heras V, Barroso A, Avendaño MS, Vazquez MJ, Castellano JM, Roa J, Tena-Sempere M. 2017. Development and validation of a method for precise dating of female puberty in laboratory rodents: The puberty ovarian maturation score (Pub-Score). Sci Rep 7:46381.

Gofur MR, Alam J, Ogawa K. 2020. Expression and localisation of ephrin-B1, EphB2, and EphB4 in the mouse testis during postnatal development. Reprod Biol 20:321-332.

Gofur MR, Ogawa K. 2019. Compartments with predominant ephrin-B1 and EphB2/B4 expression are present alternately along the excurrent duct system in the adult mouse testis and epididymis. Andrology 7:888-901.

Groten T, Fraser HM, Duncan WC, Konrad R, Kreienberg R, Wulff C. 2006. Cell junctional proteins in the human corpus luteum: changes during the normal cycle and after HCG treatment. Hum Reprod 21:3096-3102.

Hershkovitz L, Beuschlein F, Klammer S, Krup M, Weinstein Y. 2007. Adrenal 20alpha-hydroxysteroid dehydrogenase in the mouse catabolizes progesterone and 11-deoxycorticosterone and is restricted to the X-zone. Endocrinology 148:976-988.

Hirokawa N, Ishikawa H. 1974. Electron microscopic observations on postnatal development of the X zone in mouse adrenal cortex. Z Anat Entwicklungsgesch 144:85-100.

Holmes PV, Dickson AD. 1971. X-zone degeneration in the adrenal glands of adult and immature female mice. J Anat 108:159-168.

Ishii M, Nakajima T, Ogawa K. 2011. Complementary expression of EphB receptors and ephrin-B ligand in the pyloric and duodenal epithelium of adult mice. Histochem Cell Biol 136:345-356.

Kakuta H, Iguchi T, Sato T. 2018. The Involvement of Granulosa Cells in the Regulation by Gonadotropins of Cyp17a1 in Theca Cells. In Vivo 32:1387-1401.

Kania A, Klein R. 2016. Mechanisms of ephrin-Eph signalling in development, physiology and disease. Nat Rev Mol Cell Biol 17:240-256.

Kim JH, Choi MH. 2020. Embryonic Development and Adult Regeneration of the Adrenal Gland. Endocrinol Metab (Seoul) 35:765-773.

Klein R. 2012. Eph/ephrin signalling during development. Development 139:4105-4109.

Konstantinova I, Nikolova G, Ohara-Imaizumi M, Meda P, Kucera T, Zarbalis K, Wurst W, Nagamatsu S, Lammert E. 2007. EphA-Ephrin-A-mediated beta cell communication regulates insulin secretion from pancreatic islets. Cell 129:359-370.

Kullander K, Klein R. 2002. Mechanisms and functions of Eph and ephrin signalling. Nat Rev Mol Cell Biol 3:475-486.

Larson TA. 2018. Sex Steroids, Adult Neurogenesis, and Inflammation in CNS Homeostasis, Degeneration, and Repair. Front Endocrinol (Lausanne) 9:205.

Miao H, Wang B. 2009. Eph/ephrin signaling in epithelial development and homeostasis. Int J Biochem Cell Biol 41:762-770.

Miller WL, Auchus RJ. 2011. The molecular biology, biochemistry, and physiology of human steroidogenesis and its disorders. Endocr Rev 32:81-151.

Miyabayashi K, Tokunaga K, Otake H, Baba T, Shima Y, Morohashi K. 2015. Heterogeneity of ovarian theca and interstitial gland cells in mice. PLoS One 10:e0128352.

Morohashi K, Zubair M. 2011. The fetal and adult adrenal cortex. Mol Cell Endocrinol 336:193-197.

Nikolakis G, Stratakis CA, Kanaki T, Slominski A, Zouboulis CC. 2016. Skin steroidogenesis in health and disease. Rev Endocr Metab Disord 17:247-258.

Niswender GD, Juengel JL, Silva PJ, Rollyson MK, McIntush EW. 2000. Mechanisms controlling the function and life span of the corpus luteum. Physiol Rev 80:1-29.

Ogawa K, Saeki N, Igura Y, Hayashi Y. 2013. Complementary expression and repulsive signaling suggest that EphB2 and ephrin-B1 are possibly involved in epithelial boundary formation at the squamocolumnar junction in the rodent stomach. Histochem Cell Biol 140:659-675.

Ogawa K, Takemoto N, Ishii M, Pasquale EB, Nakajima T. 2011. Complementary expression and repulsive signaling suggest that EphB receptors and ephrin-B ligands control cell positioning in the gastric epithelium. Histochem Cell Biol 136:617-636.

Pasquale EB. 2005. Eph receptor signalling casts a wide net on cell behaviour. Nat Rev Mol Cell Biol 6:462-475.

Pasquale EB. 2008. Eph-ephrin bidirectional signaling in physiology and disease. Cell 133:38-52.

Pasquale EB. 2010. Eph receptors and ephrins in cancer: bidirectional signalling and beyond. Nat Rev Cancer 10:165-180.

Perez White BE, Getsios S. 2014. Eph receptor and ephrin function in breast, gut, and skin epithelia. Cell Adh Migr 8:327-338.

Pihlajoki M, Dörner J, Cochran RS, Heikinheimo M, Wilson DB. 2015. Adrenocortical zonation, renewal, and remodeling. Front Endocrinol (Lausanne) 6:27.

Rubinow KB. 2018. An intracrine view of sex steroids, immunity, and metabolic regulation. Mol Metab 15:92-103.

Sato J, Nasu M, Tsuchitani M. 2016. Comparative histopathology of the estrous or menstrual cycle in laboratory animals. J Toxicol Pathol 29:155-162.

Schaller E, Macfarlane AJ, Rupec RA, Gordon S, McKnight AJ, Pfeffer K. 2002. Inactivation of the F4/80 glycoprotein in the mouse germ line. Mol Cell Biol 22:8035-8043.

Shi W, Wang Y, Peng J, Qi S, Vitale N, Kaneda N, Murata T, Luo H, Wu J. 2019. EPHB6 controls catecholamine biosynthesis by up-regulating tyrosine hydroxylase transcription in adrenal gland chromaffin cells. J Biol Chem 294:6871-6887.

Simon DP, Hammer GD. 2012. Adrenocortical stem and progenitor cells: implications for adrenocortical carcinoma. Mol Cell Endocrinol 351:2-11.

Spencer SJ, Mesiano S, Lee JY, Jaffe RB. 1999. Proliferation and apoptosis in the human adrenal cortex during the fetal and perinatal periods: implications for growth and remodeling. J Clin Endocrinol Metab 84:1110-1115.

Stein M, Keshav S, Harris N, Gordon S. 1992. Interleukin 4 potently enhances murine macrophage mannose receptor activity: a marker of alternative immunologic macrophage activation. J Exp Med 176:287-292.

Stocco C, Telleria C, Gibori G. 2007. The molecular control of corpus luteum formation, function, and regression. Endocr Rev 28:117-149.

Uchiyama S, Saeki N, Ogawa K. 2015. Aberrant EphB/ephrin-B expression in experimental gastric lesions and tumor cells. World J Gastroenterol 21:453-464.

Walters KA, Rodriguez Paris V, Aflatounian A, Handelsman DJ. 2019. Androgens and ovarian function: translation from basic discovery research to clinical impact. J Endocrinol 242:R23-r50.

Wang Y, Shi W, Blanchette A, Peng J, Qi S, Luo H, Ledoux J, Wu J. 2018. EPHB6 and testosterone in concert regulate epinephrine release by adrenal gland chromaffin cells. Sci Rep 8:842.

Worku T, Wang K, Ayers D, Wu D, Ur Rehman Z, Zhou H, Yang L. 2018. Regulatory roles of ephrinA5 and its novel signaling pathway in mouse primary granulosa cell apoptosis and proliferation. Cell Cycle 17:892-902.

Young JM, McNeilly AS. 2010. Theca: the forgotten cell of the ovarian follicle. Reproduction 140:489-504.

Zhao C, Irie N, Takada Y, Shimoda K, Miyamoto T, Nishiwaki T, Suda T, Matsuo K. 2006. Bidirectional ephrinB2-EphB4 signaling controls bone homeostasis. Cell Metab 4:111-121.

Zirkin BR, Papadopoulos V. 2018. Leydig cells: formation, function, and regulation. Biol Reprod 99:101-111.

Zubair M, Ishihara S, Oka S, Okumura K, Morohashi K. 2006. Two-step regulation of Ad4BP/SF-1 gene transcription during fetal adrenal development: initiation by a Hox-Pbx1-Prep1 complex and maintenance via autoregulation by Ad4BP/SF-1. Mol Cell Biol 26:4111-4121.